

Power Electronic design of a Multi MW dc/dc converter

Master of Science Thesis

MIHHAIL ALIFANOV

Department of Energy and Environment
Division of Electric Power Engineering
CHALMERS UNIVERSITY OF TECHNOLOGY
Göteborg, Sweden 2013
Report No.

REPORT NO.

Power Electronic design of a Multi MW dc/dc converter

MIHHAIL ALIFANOV

Department of Energy and Environment
Division of Electric Power Engineering
CHALMERS UNIVERSITY OF TECHNOLOGY
Göteborg, Sweden 2013

Power Electronic design of a Multi MW dc/dc converter

MIHHAIL ALIFANOV

© MIHHAIL ALIFANOV, 2013.

Technical Report no.
Department of Energy and Environment
Division of Electric Power Engineering
Chalmers University of Technology
SE-412 96 Göteborg
Sweden
Telephone +46 (0)31-772 1000

Cover:
DC based windfarm with HVDC transmission

Chalmers Bibliotek, Reproservice
Göteborg, Sweden 2013

MIHHAIL ALIFANOV

Department of Energy and Environment

Division of Electric Power Engineering

Chalmers University of Technology

Abstract

- In this thesis, two topologies from a Zero voltage switching family are compared in terms of the power losses and weight of the magnetic components. These prerequisites are dictated by the purpose of the application - an offshore converter platform for an HVDC line. Two candidates were chosen: a Single active bridge dc/dc converter and a Dual active bridge dc/dc converter. The both topologies are implemented in Simulink at 2 different operating frequencies: 2 kHz and 10 kHz . The power rating of the application is 2.7 MW . The input and the output voltages are 3.6 kV and 40 kV respectively. Because of the fact that the specificity of the application does not imply a constant power supply the converters are tested in terms that they should remain in the lossless switching range even when the input power is reduced.
- The both converters have very high efficiency. The simulations have shown, that the DAB topology does not have any switching losses at all, neither in the transistors nor in the diodes. The primary side of the SAB topology operates without any switching losses in the transistors as well, though pretty high reverse recovery losses were observed in the rectifying stage. The converters performed very well with the reduced power supply and remained in the soft-switching region far below the 40 % of the nominal supply.

Index Terms: Single active bridge, Dual active bridge, dc/dc converter, lossless switching, SAB, DAB, zero-voltage switching, soft-switching, phase shifted switching.

Acknowledgements

This work has been carried out at the Department of Energy and Environment at Chalmers University of Technology.

I would like to thank the whole division of Electric Power Engineering at Chalmers and especially my examiner Prof. Torbjörn Thiringer and my supervisor Mohammadamin Bahmani for their help and support.

I dedicate this work to my beloved family.

Mihhail Alifanov
Göteborg, Sweden, 2013

Contents

Abstract	iii
Acknowledgements	v
Contents	vii
1 Introduction	1
1.1 Problem background	1
1.2 Previous work	2
1.3 Purpose	2
2 Wind Turbines	3
2.1 Fixed-speed wind turbines	3
2.2 Variable-speed wind turbine with doubly fed induction generator	4
2.3 Full variable-speed wind turbine with AC output	4
2.4 Full variable-speed wind turbine with DC output	5
3 Resonant converters	7
3.1 Series-loaded resonant dc/dc converter	7
3.2 Parallel-loaded resonant dc/dc converter	8
3.3 Hybrid-resonant dc/dc converter	9
3.4 Single active bridge dc/dc converter	10
3.5 Dual active bridge dc/dc converter	10
4 Design considerations	13
4.1 Semiconductor selection	13
4.1.1 Power diode	13
4.1.2 IGBT	14
4.2 Single active bridge	16
4.2.1 Phase shift switching	16
4.2.2 Circuit explanation	16
4.2.3 Zero voltage switching condition	19
4.2.4 Power transfer period	20
4.3 Dual active bridge	21
4.3.1 Phase shift switching	21
4.3.2 Circuit explanation	21
4.4 Transformer design	24
4.5 Resonant components	28
4.6 Output filter design	28
4.6.1 Output inductor	28
4.6.2 Output capacitor	30

5	Simulation verification	33
5.1	Simulation of Single active bridge (2, 10 kHz)	33
5.2	Simulation of Dual active bridge (2, 10 kHz)	38
5.3	Calculation of losses	40
5.4	Lossless range	41
6	Conclusions	43
6.1	Results from present work	43
6.2	Future work	43
	References	45

Chapter 1

Introduction

1.1 Problem background

Constant growth of electricity consumption in the world, limited conventional energy sources and environmental issues referred to greenhouse gas emissions and pollutions have a great impact on the development of renewable energy sources. Big hopes are put on wind power and undoubtedly this branch will expand a lot before the mankind hits the limit of conventional energy sources. Energy companies make huge investments in this sector and huge amount of wind turbines were built in the past decade. The first projects were placed in windy areas onshore. However, the best areas for wind harvesting are situated offshore and several large wind turbine parks have already been constructed in the North Sea. On one hand, it is very convenient when they are placed remotely from residential centres because in this case wind farms do not disturb people with sound pollutions, shadows or e.g their undesirable views. On the other hand, the large distances between wind power generation units and loading centres set a problem of effective and secure power transportation.

In case of underwater power transportation an HVDC lines are preferred. The main advantage over HVAC is the possibility to transmit power over long distances [6]. High voltage allows to transmit high power with relatively low current which means lower copper losses. DC-transformers are needed to reach the appropriate voltage levels. The idea is to build an HVDC line which will include a set of transformers sequentially stepping up the voltage. Hence, every transformer has an inverter on the low-voltage side to convert DC to AC and a rectifier on the high-voltage side to transform AC back to DC. Consequently, these lines can be connected to HVDC "highways" where the voltage level can reach 640 kV or higher. These extra high voltage lines may interconnect different wind harvesting regions between each other and the mainland and in this way creating a meshed system. This action enhances the system's stability due to increased redundancy. Undoubtedly, in terms of power transportation over long distances HVDC excels HVAC. The cables have lower losses, the joints are cheaper, the lengths of the lines are not limited when the HVDC systems are used [12]. However, this technology encounters another problem which does not exist in the HVAC technology. Here, the power conversion and control is accomplished with help of semiconductor switches which bring another kind of losses in to the system which are discussed in the following chapters. Briefly, every turn-on and turn-off of the transistor is accompanied by some switching losses. This events repeat hundreds or thousand times per second depending on the switching frequency of the power converter. Another type of semiconductor losses which is inherent to all electric materials is conductive and it depends on the design of the device. In case of high-power high-frequency applications where the level of currents and voltages is extremely high, the switching losses become enormous and thereby diminish the advantages of the HVDC. However, going up in frequency has its own positive aspects. High-frequency transformers with the same power rating require less inductance than their low-frequency "brothers". This means that the amount of copper and steel can be reduced and hence the size and weight. There is no need to explain that these parameters are very important in case of offshore constructions. Moreover, the switching losses can be minimised with help of different techniques or design features. Some of them are reviewed and investigated in this thesis.

1.2 Previous work

High-power converters are of great interest because they are an integral part of the rapidly evolving HVDC technology. Several works have already been aimed on the investigation of different converter topologies, trying to learn their power capabilities, design peculiarities, advantages and disadvantages of using in different applications, controllability etc. Of course, one of the main objectives of all these studies is increased efficiency of power converters. As it was already mentioned, switching losses are an undesired component of power electronic conversion. Snubber circuits and several topologies can minimise and sometimes eliminate them.

In some previous studies the possibilities of using of resonant converters were investigated. The resonant family has been known for a certain time. It has a great ability of reducing stress from the switching components and has been used a lot in e.g. portable welding equipment where high operating frequency, compact size and galvanic isolation between input and output are required. For the similar reasons, the resonant dc/dc converters were proposed for the use in offshore HVDC lines.

1.3 Purpose

The Division of electric power engineering at Chalmers University of technology is currently working on a development of high efficiency connections between offshore windfarms and the mainland. This thesis helps in finding suitable components for this project and is focused on investigation of power electronic dc/dc converters. The family of resonant converters is of great interest due to possible reduction of so-called switching losses. During the studies two promising topologies were chosen. The aim of the thesis is to design following converters:

- Single active bridge converter
- Dual active bridge converter

Prerequisites for the designs are soft-switching in a broad range of supply power and reasonable weight of magnetic components due to the offshore applications mentioned above.

Chapter 2

Wind Turbines

There are two main types of electrical systems used in wind turbines. A fixed-speed system is the oldest and the simplest one. Its main advantages are low complexity and price. However, the gearbox in this case, suffers from enormous torque variations and requires a lot of maintenance. The gearbox is one of the weakest points in any turbine.

The wind speed and wind density are never constant and they vary in time and in space. The speed of the wind high above the ground is often much higher than directly at the surface. So, in case of large sweeping areas, a tip of a blade situated in upper position will be exposed to much higher torques than the one sweeping low to the ground. The whole turbine is constantly exposed to different jolts, vibrations and torques tearing it to pieces. Undoubtedly, gentle mechanics of the gearbox suffer a lot from the effects of such stress and every failure of it increases the already high price of a megawatt produced. Moreover, the system has rather poor power quality and pollutes the network with unpleasant power pulsations. Variable-speed systems have increased the electrical complexity which gives full or partial control of the produced power. The controller adjusts the rotational speed according to the wind conditions. This action allows to reduce mechanical stress from the gearbox and significantly increases the lifetime and lowers the maintenance costs. The increased electrical complexity lowers electrical reliability and increases losses in the components. Nevertheless, such benefits as increased reliability of the gearbox, much better output power quality and control totally diminish them.

2.1 Fixed-speed wind turbines

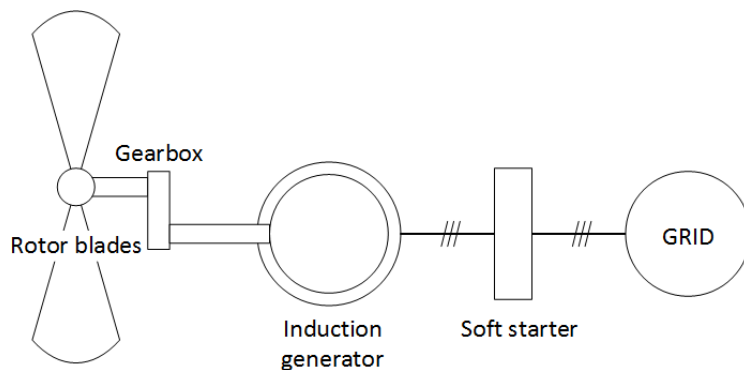


Fig. 2.1 3-phase generator with soft-starter

The simplest way to connect a wind turbine to the grid is shown in Fig. 2.1 This method is very robust, reliable and well enclosed. The generator is connected directly to the network. Since the operational frequency of the turbine cannot be changed, a gearbox helps to adjust the speed of the rotor blades in accordance with the wind speed. For the same reason, some generators are built with two sets of rotor poles to be able

to operate at two different speeds. Such arrangement requires a large amount of reactive power which is delivered by a capacitor bank. The starting current of an induction machine may be 7-10 times higher than the rated current depending on the design and a soft-starter is used to resolve this problem [7].

2.2 Variable-speed wind turbine with doubly fed induction generator

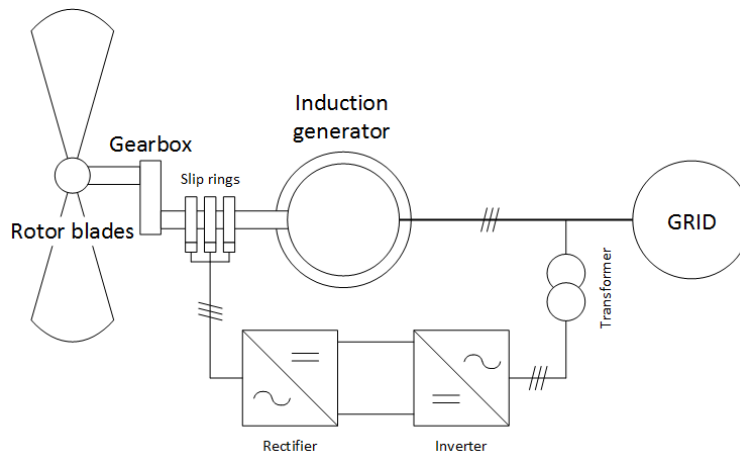


Fig. 2.2 Doubly fed induction generator wind turbine

The variable-speed wind turbine with doubly fed induction generator is shown in Fig. 2.2. This is a more advanced type of wind turbine arrangement which includes power electronics and allows the turbine to operate at variable speed. The stator windings of the induction machine are connected directly to the grid while the converter controls the rotor currents via slip rings. This allows to control the power fed to the grid independently of the rotor speed. Both active and reactive power are controlled, however the converter handles only a limited amount of the power. Nevertheless, the system has good efficiency, works in wide speed regions and withstands wind variations. A minor drawback is a need of the slip rings maintenance [7].

2.3 Full variable-speed wind turbine with AC output

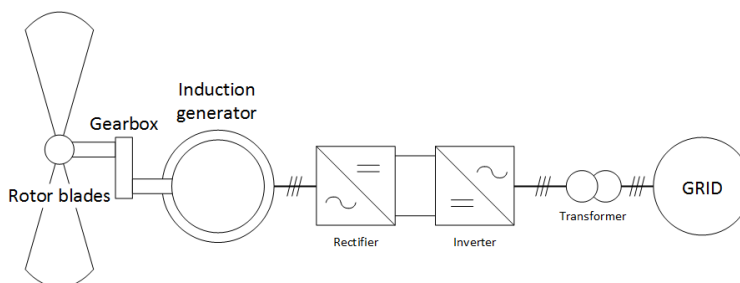


Fig. 2.3 Full variable-speed wind turbine with AC output

In Fig: 2.3 the full variable-speed wind turbine with AC output is shown. Similarly, the mechanical power from the wind blades is transferred to the rotor through the gearbox. The current is then converted from AC to DC in the rectifier and after converted back from direct to alternative in the inverter afterwards. In this case, full power produced in the wind turbine is controlled. However, this arrangement has extra losses in the semiconductors and decreased efficiency [7].

2.4 Full variable-speed wind turbine with DC output

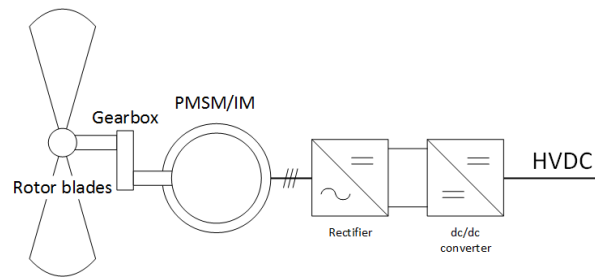


Fig. 2.4 Full variable-speed wind turbine with DC output

The full variable-speed wind turbine with DC output is shown in Fig. 2.4. This arrangement is similar to the previous one with one difference. In the output stage of the inverter a dc/dc converter is used instead. This converter is the main object of interest in this thesis. Its main ability is to step up the voltage produced in the wind turbine for connection to an HVDC line or network. The HVDC power transportation is essential for the offshore applications [7].

The investigated dc/dc converter can be used in other places in an HVDC line. In Fig. 2.5 a scheme of a windfarm based on DC voltage is depicted.

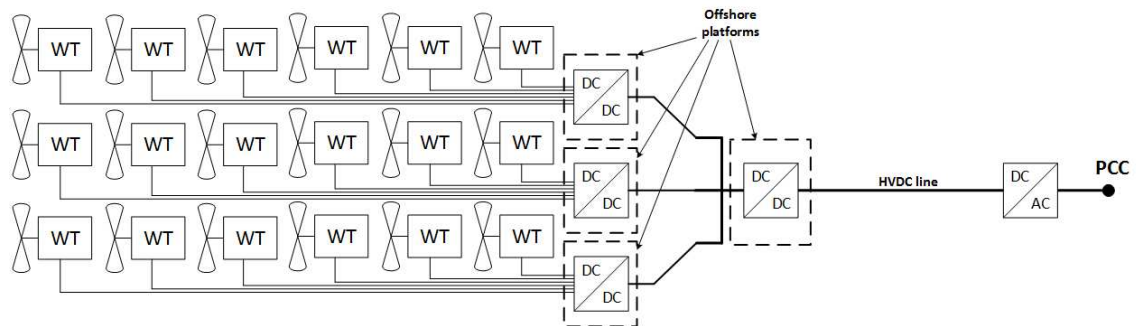


Fig. 2.5 DC based windfarm with HVDC transmission

A large number of wind turbines are harvesting energy somewhere in the sea. All the turbines are divided into several groups. In reality, one group may consist of 10-14 generating units with a separate dc/dc converter which steps up the produced voltage to a certain level. The converters are situated on platforms in the vicinity of the wind turbine arrays. Further, one more converter is needed. This dc/dc converter must be able to handle the maximum power produced by all the groups and it steps up the voltage to a new high level. After that the energy is transported via HVDC underwater cable to a dc/ac converter which is situated on the mainland and which inverts the voltage to the sinusoidal. In the point of common coupling (PCC) the system is connected to the grid.

Chapter 3

Resonant converters

In this chapter a short review of earlier studied topologies is presented. All of them belong to a resonant family of converters. These topologies utilise some form of LC resonance which helps to minimise one major drawback of conventional topologies - switching losses. Allowing, in turn, increase of the operational frequency and subsequently reduction of magnetic components.

3.1 Series-loaded resonant dc/dc converter

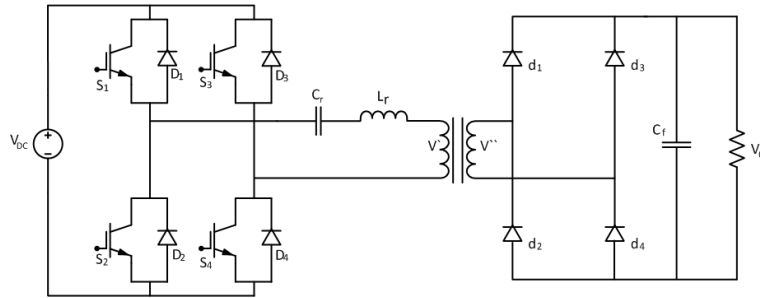


Fig. 3.1 SLR full-bridge converter

The topology of the SLR converter is shown in Fig. 3.1. It can be used in a half-bridge or a full-bridge configurations with or without a transformer. In this thesis only full-bridge topologies are reviewed. The reason is that the size of the step-up transformer is a crucial aspect for this application. In case of the full-bridge set-up the transformer is more fully utilized which is not the case for the half-bridge topology where the flux in the iron core is pushed only in one direction unless a very big capacitor is implemented on the secondary side. So, the topology includes a full-bridge inverter supplied from a DC-link, a series-resonant tank, a step-up transformer, a bridge diode rectifier and an output filter. The tank consists of a resonant inductor L_r and a resonant capacitor C_r placed in series with the output stage. The advantage of this topology that the capacitor works as a DC-blocker. A large filter capacitor C_f makes it possible to assume the output voltage to be pure DC. Hence, the device is suitable for high-voltage low-current applications. The resonant frequency of the LC-tank is given by

$$\omega_0 = \frac{1}{\sqrt{L_r C_r}} = 2\pi f_0 \quad (3.1)$$

The current through the resonant inductor and the voltage across the resonant capacitor can be described by the functions:

$$i_L(t) = I_{L0} \cos \omega_0(t - t_0) + \frac{V_d - V_{c0}}{Z_0} \sin \omega_0(t - t_0) \quad (3.2)$$

$$v_c(t) = V_d - (V_d - V_{c0}) \cos \omega_0(t - t_0) + Z_0 I_{L0} \sin \omega_0(t - t_0) \quad (3.3)$$

The SLR topology naturally works only as a step-down converter. Because of this, the step-up transformer is used to be able to increase the output voltage. The SLR converters are effective at light loads, because the current in the device decreases when the load drops. However, the output voltage is uncontrollable at no-load conditions which is a big drawback. There are different control strategies that can be used for the SLR converters. The most widely used strategy is frequency modulation. In this case, the transformer and the output filter cannot be optimised due to the variations in operating frequency and this is also a very important drawback [8] [4]. There are three operating modes used with the SLR topology.

- Discontinuous-Conduction Mode

DCM is achieved when the switching frequency is lower than half of the resonant frequency $f_s < \frac{f_r}{2}$. In this case, the turn off occurs at zero voltage and zero current. The converter operates as a current source because the output current I_o stays constant despite the variations in the output voltage V_o . The turn on happens only at zero current and voltage has a finite value. Nevertheless, there are no switching losses in this mode. However, the current through the inductor has rather high peak values which leads to increased conduction losses [8].

- Continuous-Conduction Mode with $\frac{f_r}{2} < f_s < f_r$

In this continuous-conduction mode, the switching frequency of the converter varies between the resonant frequency and the half of it. The switches turn off naturally at zero voltage and zero current. However, there are switching losses because turn on of the transistors occurs at a finite current and voltage [8].

- Continuous-Conduction Mode with $f_s > f_r$

In this continuous conduction mode the switching frequency is higher than the resonant frequency. Here, it is opposite to the previous case, the turn on is lossless due to zero current and zero voltage across the switches and the turn off occurs at a finite current [8].

3.2 Parallel-loaded resonant dc/dc converter

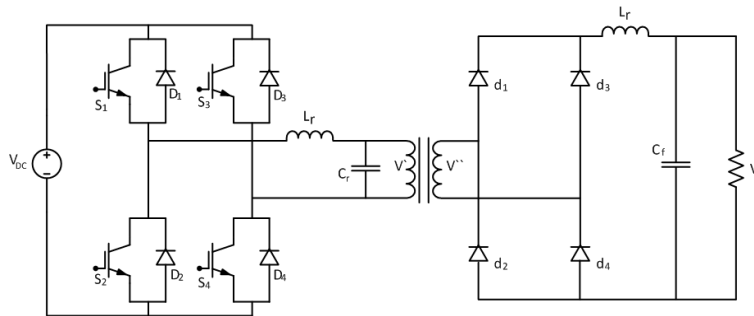


Fig. 3.2 PLR full-bridge converter

This topology is similar to the SLR converter but with one difference in the resonant tank. The resonant capacitor is situated in parallel with the output resistance. This difference allows to control the output at the no-load condition but the DC-blocking capacitor option disappears. Unlike the SLR topology, the efficiency of the converter becomes worse if the load decreases. The PLR converter can both step up and step down the output voltage without using the transformer and it behaves as a voltage source. The output current at high switching frequencies can be assumed ripple-free if a large inductor is chosen for the output filter. [8] [4]

$$i_L(t) = I_0 + (I_{L0} - I_0)\cos\omega_0(t - t_0) + \frac{V_d - V_{c0}}{Z_0}\sin\omega_0(t - t_0) \quad (3.4)$$

$$v_c(t) = V_d - (V_d - V_{c0})\cos\omega_0(t - t_0) + Z_0(I_{L0} - I_0)\sin\omega_0(t - t_0) \quad (3.5)$$

- Discontinuous-Conduction Mode

In this mode both i_L and v_c are equal to zero for some time. The output voltage is controlled by

changing this interval. As the converter operates in the DCM, the current through the inductor naturally dies out causing lossless turn-off of the switches. The turn-on is also without losses because it starts at both zero voltage and current. As in the case with the SLR, this mode has high peak values of i_L , which means high conduction losses. [8]

- Continuous-Conduction Mode

If the switching frequency is below the resonant one, the transistors turn on at a finite voltage and current. However, turn-off is lossless because it happens naturally at zero current when i_L reverses its direction. [8]

- Continuous-Conduction Mode

This mode is achieved when $f_{sw} > f_r$. The turn-on is lossless because it occurs at zero current, while turn-off requires a snubber circuit since the current through the switch is interrupted at a finite value. [8]

3.3 Hybrid-resonant dc/dc converter

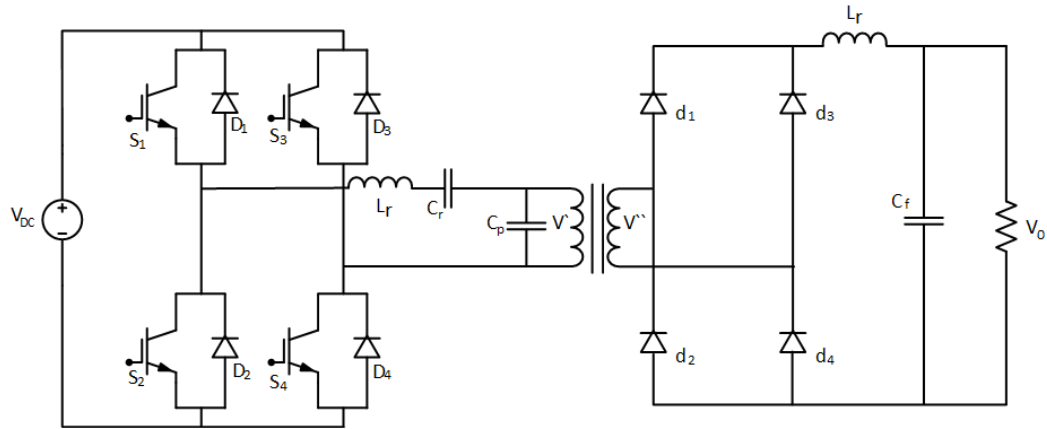


Fig. 3.3 ZVS full-bridge converter

The full-bridge hybrid-resonant converter is shown Fig. 3.3. The topology can be used in half-bridge configurations as well and is a combination of both the SLR and the PLR topologies. Here, the resonant tank has capacitors both in series and in parallel with the output stage. Both capacitances can be external elements or parasitic t.ex. capacitance of the transformer winding. The converter combines the characteristics of the two previous topologies. Interestingly enough, that such arrangement takes the good things from the SLR and the PLR converters, diminishing some of shortcomings. The converter can be used both in step-up and step-down applications, it is naturally short-circuit proof and has a DC-blocking capacitor. A wide range of soft switching can be achieved, by proper control design such a converter always perform better than the equivalent PLR or SLR configurations. However the best performance is possible only in specific frequency region. A configuration of such converter can be characterised by the ratio of series-to-parallel inductances. [4]

$$A = \frac{C_p}{C_r} \quad (3.6)$$

In a converter with a low A ratio the properties of the series-loaded converter dominate and vice versa, a design with high ratio behaves like the PLR. However, the operating frequency also changes the behaviour of the converter. It operates as a PLR at high frequencies and as a SLR at low frequencies. It has better control characteristics than the SLR or the PLR have, and the output voltage is controllable under no-load condition. The current ripple in the output filter is rather low. However, there are some drawbacks that are common for the whole family. The best performance is obtained in a narrow region, the main current has high peak and rms values, which leads to increased conduction losses. Another thing is that the passive elements in the LCC topology sometimes should be physically larger to withstand high peak voltage over the capacitor bank which is not the case for the SLR topology. [8] [4]

3.4 Single active bridge dc/dc converter

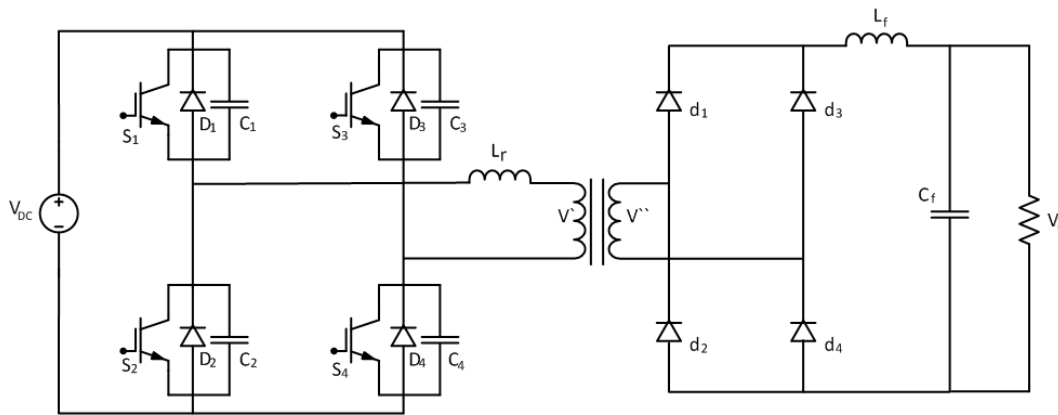


Fig. 3.4 ZVS full-bridge converter

The Single active bridge or Zero-voltage-switching dc/dc converter is from a family of resonant-switch converters. The resonant tank in such converters is used for a voltage shift or a current change in the switch to minimise the switching losses. Judging by the name, one can guess that the voltage is shaped in this kind of device. The layout of it is similar to the single-phase full-bridge topology. It consists of a transformer, a full-bridge single phase inverter connected to the primary side of the transformer and a diode bridge rectifier on the secondary side. However, the full-bridge topology needs some modifications to be named zero-voltage switched. The ZVS technique also requires a resonant tank which establishes zero-voltage across the transistor before it turns on. As in the previous cases, the leakage inductance of the transformer can be utilised in the resonant tank to initialise the zero-voltage switching. This feature allows to reduce the switching losses significantly. The result is that the converter can operate at higher frequencies and will still be in the safe thermal region. As was mentioned in the introduction, a higher operating frequency allows to reduce the size of the transformer. A real converter has a lot of other reactive elements such as stray inductances in the circuit or a magnetizing inductance of the transformer which influence on the behaviour of the converter a lot, especially at high frequencies. In this thesis, the resonant inductance represents the lump of all possible inductances in the primary circuit. The second basic element of any resonant tank is the capacitor. Very often, the parasitic capacitance of the switching elements is used for this purpose. However, low power IGBTs have rather low capacitance. In this case, extra capacitor snubbers need to be placed across the switches. [4]

3.5 Dual active bridge dc/dc converter

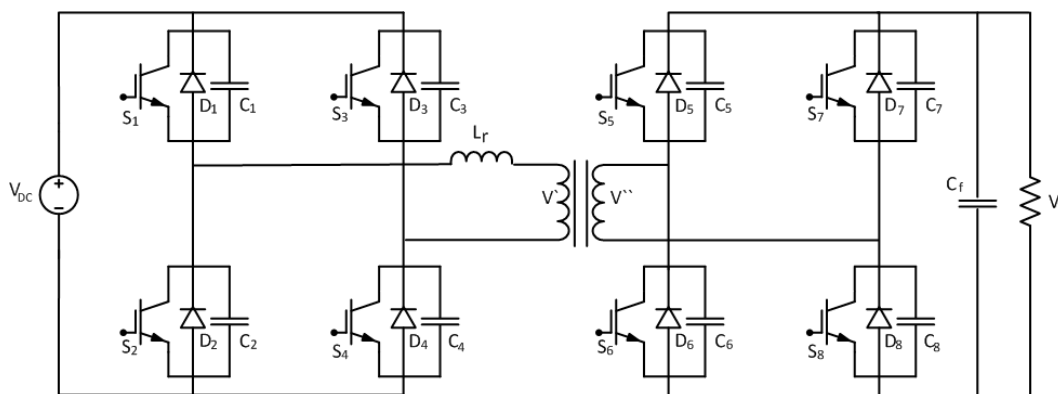


Fig. 3.5 DAB full-bridge converter

The topology is depicted in Fig. 3.5 and it consists of eight active components. Four switches are placed on the primary side and four other switches replace the rectifier diodes from the previous topology. The leakage

inductance of the transformer is utilised in the same manner as in the case of the ZVS full-bridge converter. The power can flow in the both directions and such a converter can operate as step-up or step-down topology. The main advantage of the DAB converters are control simplicity, low number of passive components and ideally no switching losses without any increase of the conduction losses. It is easy to optimise the transformer and output filter because the converter operates at constant frequency. However, there is a need of a large capacitor in the output stage because the converter produces a high ripple current. [4]

Chapter 4

Design considerations

4.1 Semiconductor selection

Semiconductors are the base of any power electronic converter. These elements allow to change the conductance of a circuit from negligibly small values to a very high values comparable with the electric conductors. With right control techniques it is possible to shape voltages and currents to achieve the desired results. There are two types of semiconductors that are used in this work. All the components are required to withstand high voltage. The converter ratings are:

- Input voltage $V_{DC} = 3600V$
- Input current $I_{in} = 750A$
- Output voltage $V_o = 40000V$
- Output current $I_o = 67.5A$

4.1.1 Power diode

Power diodes are an essential part of almost any converter. This semiconductor device passes current through in one direction while it blocks in another direction. The symbol of a diode is depicted in Fig. 4.1a. Current flows from the positive electrode called anode to the negatively charged electrode called cathode. In Fig. 4.1b typical I-V characteristic of a power diode is shown.

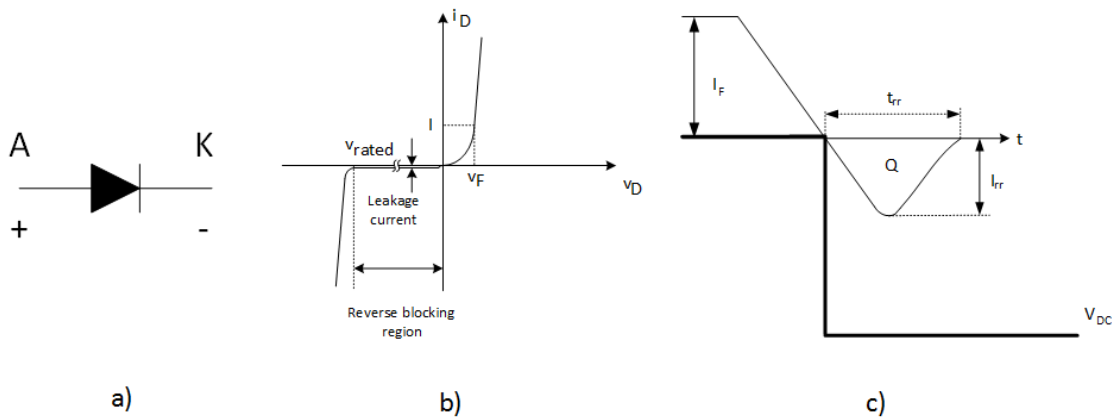


Fig. 4.1 (a) Diode symbol (b) I-V characteristic of a diode (c) reverse recovery of a diode

In the first quadrant the diode is forward biased. In another words, the polarity of the applied voltage coincides with the polarity of the diode. Forward current is always accompanied with some voltage drop which grows if the current increases. Reverse biased characteristic is situated in the third quadrant where the applied voltage is negative. Only some leakage current passes through in this mode. However, the leakage

current is so small that it can be neglected in most of the cases. Every diode is characterised by the voltage it can withstand which is called rated voltage V_{rated} or breakdown voltage V_{BD} . Above this voltage, the impact ionisation starts inside the device and the electron avalanche destroys it. [8].

A very important interval of a power diode operation is depicted in Fig. 4.1c. It is called a reverse recovery and it occurs when a power diode turns off. Every time a power diode is forward biased, a large amount of electrons and holes leave their home areas and travel into neighbourhood regions and when the reverse voltage is applied, it takes the time t_{rr} for them to get back to the n- and p-regions respectively for the recombination. This event is represented by the negative current on the picture. If there is a voltage applied after the turn-off the area bounded by the negative current becomes a loss.

In this thesis, power diodes are used as freewheeling diodes across the switches and compose the rectifying part of the SAB converters. The output voltage of the converter is 40 kV. A standard rule of thumb in power electronics for breakdown voltages is 10%. So, each of the four rectifier diodes should withstand 44 kV and be able to conduct half of the output current in forward bias mode which is 33.75 A. The 5SLX 12M6520 power diode from ABB was chosen for this purpose. One such diode is designed to handle 3600 V average reverse voltage and 50 A forward current. A set of 12.22 diodes is required in order to build a diode that can withstand 44 kV average reverse voltage.

Very often transistor modules have inbuilt freewheeling diodes. In all simulations such modules were used on the primary side. However, in case of a DAB converter, the freewheeling diodes and switches on the secondary side were chosen separately due to absence of complete modules with required power ratings. Therefore, the model 5SLY 12N4500 was chosen for this role. This diode is made to handle 2800 V average reverse voltage. Therefore, a set of 15.71 such diodes are required to withstand 44 kV reverse voltage.

- Conduction losses are the losses that are caused by an inherent forward resistance of the diode. R_{on} is non-linear and changes with respect to the forward current strength I_F . Where, a lower current causes a higher resistance and hence, higher losses per ampere. The average power dissipated in the diode during a conduction can be found if the average current and the average voltage drop across the device are known. Both of them can be found by integrating the curves during the on-state:

$$P_{cond,diode} = I_F V_F = \frac{1}{T_s} \int_0^{t_{on}} (v_F(t) i_F(t)) dt \quad (4.1)$$

- Reverse recovery losses can be found from the datasheet if the forward current I_F is known

4.1.2 IGBT

The IGBT is a voltage-controlled semiconductor device. The symbol and volt-ampere characteristic are depicted in Fig. 4.2(a). This types of devices are widely used in power electronics due to low on-state voltage drop even in devices with high blocking voltage levels. [8]

The IGBT is a voltage controlled device with a high gate impedance which means that it requires only little energy to switch it. Forward volt-ampere characteristic is shown the first quadrant in Fig. 4.2(b). It is seen that the amount of current passing through the device can be changed by regulating the voltage between the gate and emitter(source) V_{GS} . The characteristics are mostly linear but when the regulating voltage approaches threshold level $V_{GS,(th)}$, only very little current passes through the device. [8]

In this thesis, two different IGBT models are used. The primary bridges are identical for the both topologies and consist of the modules 5SNA 0750G650300 from ABB. These are the most powerful IGBTs on the market so far. The secondary side of the DAB converters is built on 5SMY 12N4501. One such module can withstand 2800 V average reverse voltage. Therefore, a module equivalent to 15.71 such transistors is required to withstand 44 kV reverse voltage.

IGBTs have also two type of losses:

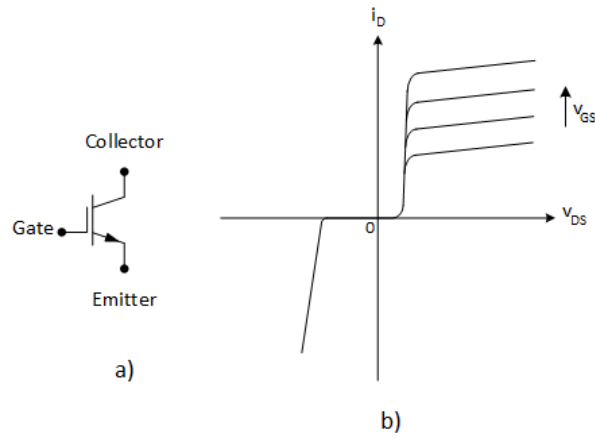


Fig. 4.2 (a) IGBT symbol (b) I-V characteristic of an IGBT

- Switching losses can be determined from the switching waveform of a transistor. An example is shown in Fig. 4.3.

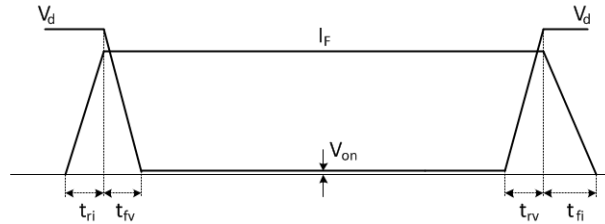


Fig. 4.3 IGBT switching waveform

Two triangular areas which are bounded by the voltage and the current curves represent the dissipated switching energy per one period. The area of the left triangle is equal to energy during turn-on transient

$$W_{c(on)} = \frac{1}{2} V_d I_c t_{c(on)} = \frac{1}{2} V_d I_c (t_{ri} + t_{fv}) \quad (4.2)$$

and the right triangle represents the turn-off energy

$$W_{c(off)} = \frac{1}{2} V_d I_c t_{c(off)} = \frac{1}{2} V_d I_c (t_{rv} + t_{fi}) \quad (4.3)$$

Here, t_{ri} and t_{rf} stand for the current rise and fall times, while t_{rv} and t_{rf} are the voltage rise and fall times. All these parameters are usually written in the datasheets. Then, the total power lost due to switching transitions can be calculated, using

$$P_{sw} = \frac{1}{2} V_d I_c (t_{rv} + t_{fi}) \quad (4.4)$$

- The conduction losses are found similarly as in case of a power diodes. The average power can be easily found if the average collector current and the average voltage drop between collector and emitter are known

$$P_{cond,IGBT} = I_c V_{CE} = \frac{1}{T_s} \int_0^{t_{on}} (v_{CE}(t) i_C(t)) dt \quad (4.5)$$

Graphically, this loss is represented by a small rectangular area under the voltage curve between two rectangles. In reality, the voltage drop across the device changes non-linearly in response with the current and this area obtains a complex trapezoidal form.

4.2 Single active bridge

4.2.1 Phase shift switching

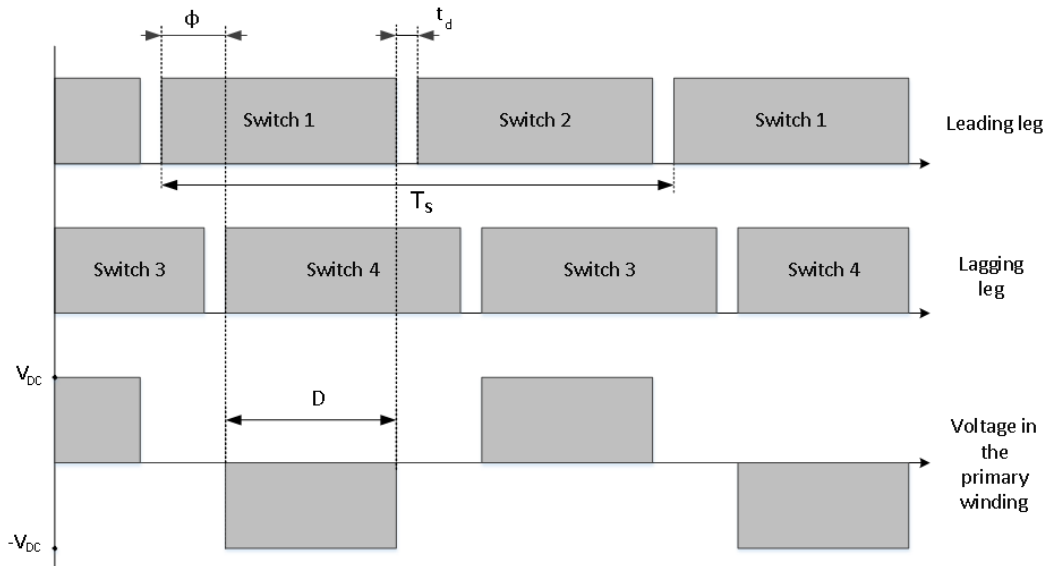


Fig. 4.4 Control pulses in a phase shifted switching.

Phase shifted switching is an important and specific part of the ZVS technique. In the convenient full-bridge converter topology the switches turn on and off diagonally. Each diagonal pair of transistors conducts maximum half a cycle before the second pair of transistors switch in. Furthermore, the ratio between the output and the input voltages is proportional to the conduction time of the diagonal pairs.

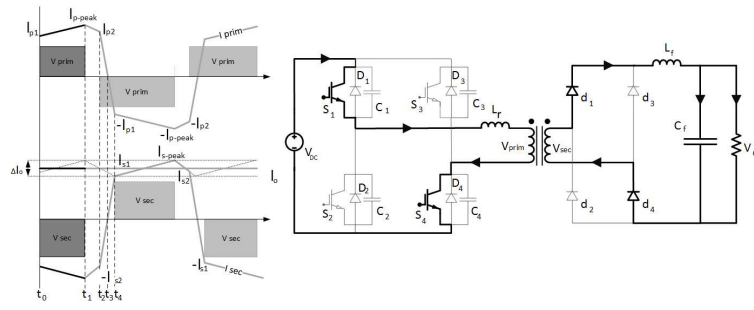
In case of phase shifted switching, the control pulses of the transistors are kept the same, usually about half a cycle. However, it is not equal to the conduction time of the transistors. While the switch is being closed, the current flows through the freewheeling diode and only then commutates the transistor itself. The operational principle is depicted in Fig. 4.4. A pair of transistors which are placed in series form a leg. One leg is called leading and it consists of the switches S_1 and S_2 , another leg is called lagging and the switches S_3 and S_4 form it. A small delay or a dead time t_d between the conduction is introduced to prevent short circuiting of the DC-link through the series connected transistors. In another words, the current through one switch must fully die out before another transistor situated on the same leg can start to conduct. As a result, the conduction time of one switch is slightly shorter than a half of the period. Of course, t_d can be increased, making the conduction time shorter but in case of high power applications the costly switches are meant to be utilized as much as possible and t_d is kept to be as short as possible. The voltage across the primary winding of the transformer is changed by controlling a phase shift angle ϕ . An increase in the phase angle will lower the voltage across the winding and vice versa smaller ϕ causes higher voltage in the transformer. The length of one voltage pulse can be easily derived from Fig. 4.4 as

$$t_{pulse} = D * \frac{T_s}{2} = T_s - 2 * t_d - \frac{\phi}{360^\circ} \quad (4.6)$$

The amplitude of the voltage across the primary winding swings between V_d and $-V_d$.

4.2.2 Circuit explanation

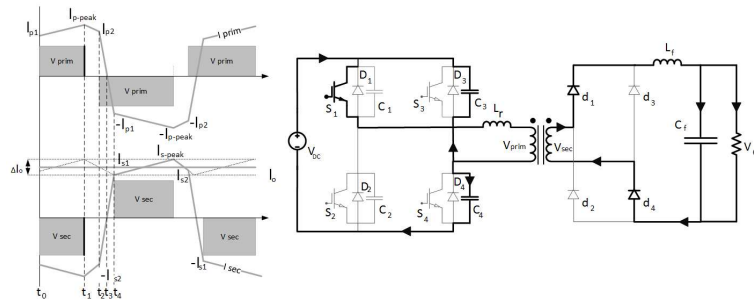
As it was mentioned above, the processes that are common for the ZVS technique differ a lot from the conventional switching technique. Power transfer is regulated by the phase shift between two transistor legs. Another important aspect is the utilization of the resonant elements in the circuit. A detailed explanation of the processes typical for the ZVS full-bridge converter is given below. The explanation covers one half-cycle in CCM.

Fig. 4.5 SAB. Power transfer interval $t_0 < t < t_1$

$t_0 < t < t_1$ • A power transfer interval is shown in Fig. 4.5. Two diagonal switches S1 and S4 are closed and two others are open. The converter works just like in the case of the conventional full-bridge topology. The supply voltage V_d is maintained across the transformer and the current in the primary winding of the transformer rises from I_{p1} to I_{p-peak} . The steepness of the slope is defined by the inductance in the circuit. The resonant inductance is much lower than the inductance of the output filter and thus can be neglected. Hence, the slope of the current in the primary is given by

$$\frac{\partial I_p}{dt} = \frac{V_d - nV_o}{nL_f} \quad (4.7)$$

where V_d is the DC-link voltage, I_p is the current in the primary winding, V_o is the output voltage and L_f is the filter inductance. The last two values should be scaled down by the transformer ratio n .

Fig. 4.6 SAB. Right leg resonant transition $t_1 = t$

$t = t_1$ • The right leg resonant transition is shown in Fig. 4.6. At time t_1 the switch S_4 opens and the resonant transition in the right leg occurs. The voltage across the primary windings drops almost momentarily to zero. The main current which flew through two diagonal switches and the primary winding does not stop immediately but it gets redirected into the capacitor C_4 . This action provides lossless turn-off of the switch S_4 . During the transition, the capacitance of the switch S_4 gets charged until the level of the supply voltage V_d . Meanwhile, the voltage across the switch S_3 decreases to zero volts which makes it possible to turn on the device without the losses. When the voltage at the transformers primary winding drops from V_d to zero, at some point it gets lower than $V_o n$. At this instant the output inductor starts to supply the main current until there is no voltage across L_r at all.

The whole transition process occurs very fast because it lasts only until both of the capacitors get recharged:

$$t_{transition} = \frac{(C_3 + C_4)V_{DC}}{I} \quad (4.8)$$

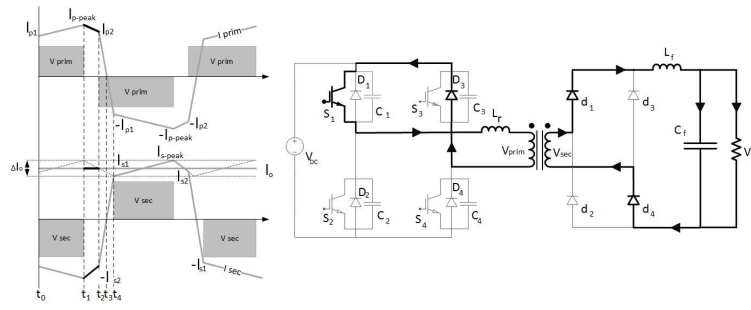


Fig. 4.7 SAB. Clamped freewheeling interval $t_1 < t < t_2$

$t_1 < t < t_2$ • A clamped freewheeling interval is depicted in Fig. 4.7. Here, the main current freewheels through the closed switch S_1 and the forward-biased diode D_3 . Its value decreases from the peak value I_{p-peak} to a value of I_{p2} . The current is not supplied from the DC-link. The rate of change is defined by the inductance in the circuit. Again, the resonant inductance is neglected:

$$\frac{\partial I_p}{\partial t} = -\frac{nV_o}{nL_f} = -\frac{V_o}{L_f} \quad (4.9)$$

The voltage across the capacitor C_3 is still equal to zero and the switch S_3 can be turned on at any time. If power MOSFETs are used as the switches, some part of the current will flow through the transistor in reverse direction (source to drain), the another part continues to flow through the body diode D_3 . IGBTs cannot conduct in reverse direction and the whole current flows through the diode D_3 .

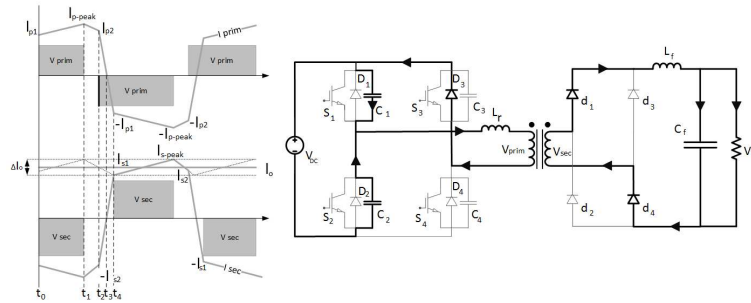


Fig. 4.8 SAB. Left leg resonant transition $t_2 = t$

$t = t_2$ • The left leg resonant transition is shown in Fig. 4.8. At t_3 the switch S_1 is turned off and the current continues to flow through the output capacitance C_1 , the primary winding and the parallel impedances of S_3 and D_3 . The voltage across S_1 increases and the drain to source voltage of the switch S_2 decreases and when it reaches zero, the transistor can be turned on without losses. At the instant when the voltage across C_2 gets higher than the voltage across the leakage inductance, all four diodes in the rectifier get forward-biased and the secondary winding becomes short-circuited.

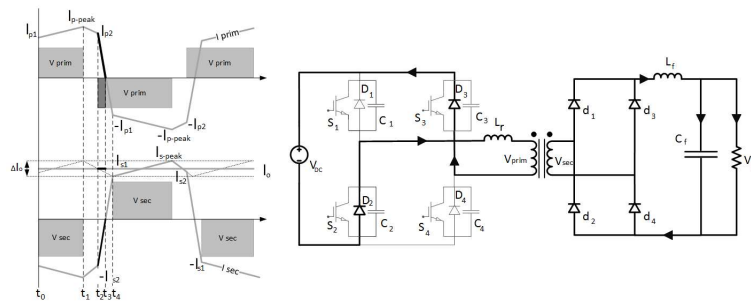


Fig. 4.9 SAB. Freewheeling interval $t_2 < t < t_3$

$t_2 < t < t_3$ • The left leg resonant transition is continued in Fig. 4.9. Directly after t_2 the capacitors C_1 and C_2 are recharged. The main current flows in reverse direction through the freewheeling body diodes D_2 and D_3 which are forward biased now. The transistors S_2 and S_3 can be turned on at any instant and the ZVS condition will be satisfied because its drain to source voltage equals to zero volts. The secondary winding is still short circuited. The rate of change of the main current is given by:

$$\frac{\partial I_p}{dt} = -\frac{V_{DC}}{L_r} \quad (4.10)$$

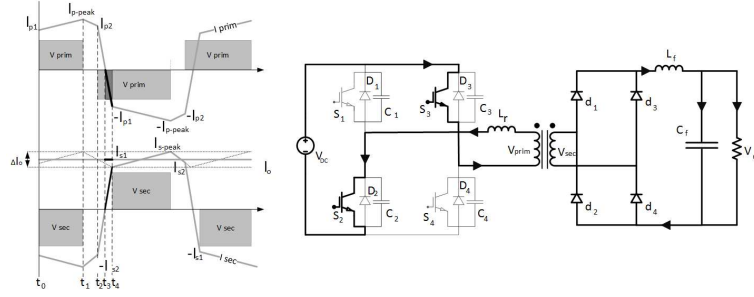


Fig. 4.10 SAB. Power transfer interval with a short-circuited secondary side $t_3 < t < t_4$

$t_3 < t < t_4$ • The main current reverse can be seen on Fig. 4.10 and the switches S_2 and S_3 turn on. The time when the switch S_3 is going to be turned off defines the ratio between the input and output voltages. At time t_4 the current through the diodes D_1 and D_4 fully dies out and the output filter can start to store energy again. [2]

4.2.3 Zero voltage switching condition

As it was mentioned before, zero-voltage switching requires special conditions to be able to occur. The trick is that the energy stored in the resonant inductor just before the transition must be greater than the energy stored in the resonant capacitor. Hence, the zero-voltage transition prerequisite can be written as

$$E = \frac{1}{2} L_r I_{p2}^2 > \frac{1}{2} C_r V_{DC}^2 \quad (4.11)$$

Thus, the critical magnitude of the current that satisfies zero-voltage transition can be calculated from

$$I_{p2-critical} = V_{DC} \sqrt{\frac{C_r}{L_r}} \quad (4.12)$$

However, the waveform on the current strongly depends on the load current. And at light loads the ZVS full-bridge converters often go over to hard-switching mode. To find the critical value of the load current we can take a look at the transformer current waveforms in Fig. 4.11. It is obvious from the topology that the load current is just the rectified waveform of the current passing through the secondary winding of the transformer. Hence, geometrically from the waveform it is possible to obtain I_{s2} since the current slope:

$$I_{s2} = I_{s-peak} - \frac{V_o}{L_o} (1 - D) \frac{T_s}{2} \quad (4.13)$$

As it is seen from the picture, the waveform of the secondary current looks exactly the same as the current in the primary. However, to find any value of the primary current at some instant of time, the secondary current should be multiplied with the transformer ratio.

$$I_{p2} = \frac{N_2}{N_1} I_{s2} = \frac{N_2}{N_1} \left(I_{s-peak} - \frac{V_o}{L_o} (1 - D) \frac{T_s}{2} \right) \quad (4.14)$$

Substituting I_{p2} with $I_{p2-critical}$ from (4.12) the minimum value of the load current can be obtained:

$$I_o \geq \frac{N_1}{N_2} V_{DC} \sqrt{\frac{C_r}{L_r}} - \frac{\Delta I_o}{2} + \frac{V_o}{L_o} (1 - D) \frac{T_s}{2} \quad (4.15)$$

A smaller load current will force the converter to leave the lossless region [11].

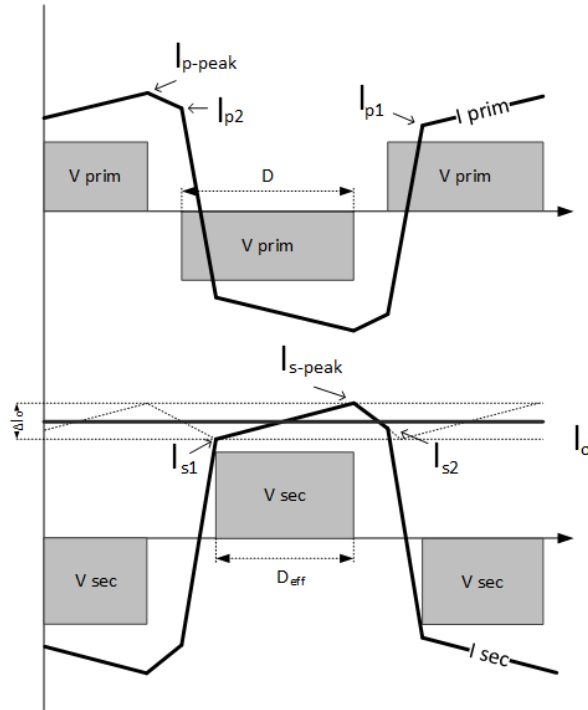


Fig. 4.11 Transformer curves

4.2.4 Power transfer period

The currents and voltages across the both transformer windings are shown in Fig. 4.11. It is clearly seen that the secondary voltage duration is slightly shorter from the primary and it depends on the main current. The secondary voltage pulse is somewhat shorter and denoted as D_{eff} . The subscript stands for effective since this value defines the conversion ratio of the converter:

$$\frac{V_o}{V_{DC}} = D_{eff} \frac{N_2}{N_1} \quad (4.16)$$

where N_1 and N_2 represent the number of turns in the transformer. It is clearly seen from the picture that the voltage across secondary winding is applied for a slightly shorter period of time ($D_{eff} < D$). Hence, this effective period when the actual energy transfer occurs can be expressed as

$$D_{eff} = D - \Delta D \quad (4.17)$$

As it seen from Fig. 4.11 ΔD is equal to a period while the main current drops from I_{p2} to $-I_{p1}$ or rises from I_{p1} to $-I_{p2}$. The slope of the current is given in (4.10). Thus it can be defined as

$$\Delta D = \frac{I_{p1} + I_{p2}}{\frac{V_{DC} T_s}{L_r} \cdot 2} \quad (4.18)$$

The load current waveform repeats the behaviour of the primary current in the time section $t_0 < t < t_1$. Thus, I_{p1} can be written as

$$I_{p1} = \frac{N_2}{N_1} \left(I_o - \frac{\Delta I_o}{2} \right) \quad (4.19)$$

I_{p2} was derived in previous section and ΔD can be obtained by inserting (4.14), (4.19) into (4.18)

$$\Delta D = \frac{\frac{N_2}{N_1} (2I_o - \frac{V_o}{L_o} (1-D) \frac{T_s}{2})}{\frac{V_{DC} T_s}{L_r} \cdot 2} = \frac{4L_r I_o}{nV_{DC} T} - \frac{L_r V_o}{nV_{DC} L_o} + \frac{L_r V_o D}{nV_{DC} L_o} \quad (4.20)$$

where $n = \frac{N_1}{N_2}$. Now, D can be evaluated by combining (4.16), (4.20) with (4.17) :

$$D = \frac{\frac{nV_o}{V_{DC}} + \frac{RL_r I_o}{nV_{DC} T} - \frac{L_r V_o}{nV_{DC} L_o}}{\frac{nV_{DC} L_o - L_r V_o}{nV_{DC} L_o}} = \frac{nV_o + \frac{4L_r I_o}{nT_s} - \frac{L_r V_o}{nL_o}}{V_{DC} - \frac{L_r V_o}{nL_o}} \quad (4.21)$$

And finally, by inserting (4.20) into (4.17):

$$D_{eff} = D - \Delta D = D - \frac{4L_r I_o}{nV_{DC}T} + \frac{L_r V_o}{nV_{DC}L_o} - \frac{L_r V_o D}{nV_{DC}L_o} \quad (4.22)$$

And substituting several terms with expressions from (4.16)

$$D_{eff} = D - \frac{4L_r I_o D_{eff}}{n^2 V_o T_s} + \frac{L_r D_{eff}}{n^2 L_o} - \frac{L_r D D_{eff}}{n^2 L_o} \quad (4.23)$$

the effective duty cycle of the converter can be found by

$$D_{eff} = \frac{D}{1 + \frac{4L_r I_o}{n^2 V_o T_s} - \frac{L_r}{n^2 L_o} + \frac{D L_r}{n^2 L_o}} \quad (4.24)$$

(4.24) can be reduced by neglecting the term $\frac{L_r}{n^2 L_o}$ since it is small comparing to others and $\frac{V_o}{I_o}$ can be changed by R_o

$$D_{eff} = \frac{D}{1 + \frac{4L_r}{n^2 R_o T_s}} \quad (4.25)$$

The obtained value D_{eff} represents the duty cycle of the secondary winding of the transformer. [11]

4.3 Dual active bridge

4.3.1 Phase shift switching

The switches in the DAB topology operate at constant speed. They switch diagonally with 50% constant duty cycle which allows to utilise the transistors fully. The converter can be supplied from both sides. In this thesis, the power is supplied only from the low voltage side. So, the low-voltage bridge consists of two different modes $S_1 S_4$ and $S_2 S_3$ which create rectangular voltage pulses resulting in an alternating square wave across the primary winding of the transformer. The high-voltage switches are controlled in a similar way. However, the control impulses are phase shifted in accordance with the low-voltage side. The phase shift is specified by an angle ϕ . The power transfer is regulated by controlling this angle and the sign of it defines the direction of the power flow. A positive sign allows the power to flow from low-voltage side to high-voltage side and vice versa negative sign results in reverse flow direction. The maximum power transfer is achieved when the angle equals to 90° or -90° depending on the direction of the power flow. However, the second case is irrelevant for the thesis. The product of these two phase shifted voltages is a voltage across the leakage inductance V_r .

In the following description one positive half-cycle is explained:

4.3.2 Circuit explanation

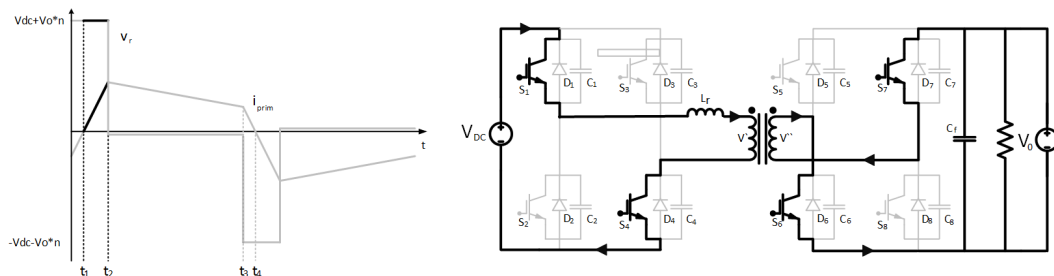


Fig. 4.12 DAB. Power transfer period. $t_1 < t < t_2$

$t_1 < t < t_2$ • The switches S_1 and S_4 are closed on the primary side while S_6 and S_7 conduct on the secondary side. Since the switches are closed on both sides, the leakage inductance becomes short-circuited between two voltage sources and the main current through the transformer windings rapidly increases:

$$\frac{\partial i_1}{dt} = \frac{V_{DC} + V_o/n}{L} \quad (4.26)$$

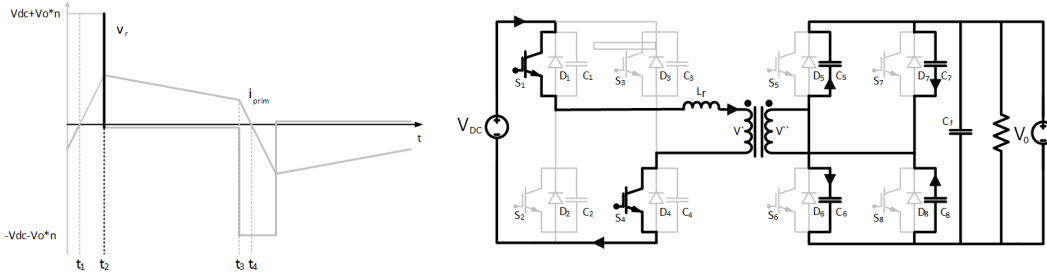


Fig. 4.13 DAB. Secondary side resonant transition $t = t_2$

$t = t_2$ • The capacitors across the switches S_6 and S_7 were previously discharged, while the voltage across C_5 and C_8 is equal to the upper voltage rail V_o . So, when the switches open at $t = t_2$, the secondary current continues to flow through all the capacitors located on the secondary side. C_6 and C_7 get charged, providing lossless turn-off of the switches S_6 and S_7 , while C_5 and C_8 get discharged putting the voltage across the switches S_5 and S_8 equal to zero. The nature of this event is similar to the resonant transitions described before.

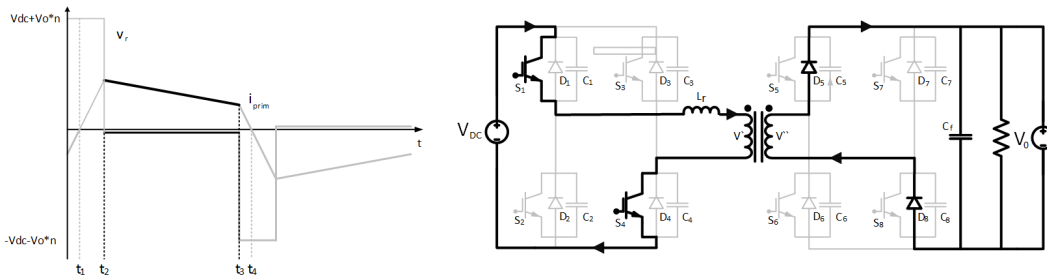


Fig. 4.14 DAB. Freewheeling interval $t_2 < t < t_3$

$t_2 < t < t_3$ • After the recharge, the voltage V_r becomes equal almost to zero, though V_{DC} and $-V_o/n$ cancel out each other. All the switches on the secondary side are open and the diodes D_5 and D_8 conduct and it operates just like a rectifier bridge. The primary current changes at the following rate:

$$\frac{\partial i_2}{dt} = \frac{V_{DC} - V_o/n}{L} \quad (4.27)$$

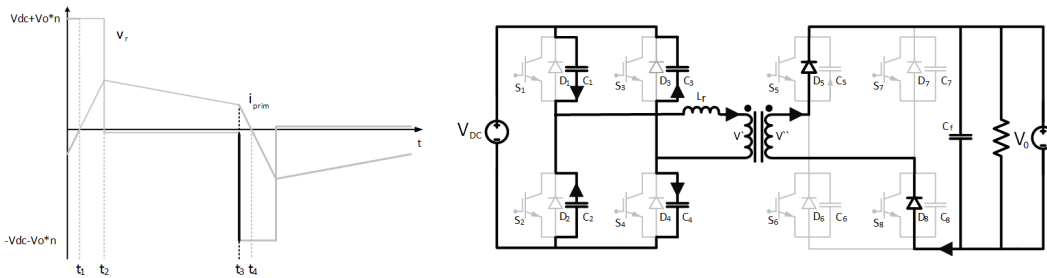


Fig. 4.15 DAB. Primary side resonant transition $t = t_3$

$t = t_3$ • Another resonant transition occurs, but this time on the primary side. When the switches S_1 and S_4 opened, the main current rushes into the capacitors. C_1 and C_4 get charged to V_{DC} providing soft-switched turn-off of the above-stated transistors. C_2 and C_3 get discharged paving the way for lossless turn-on of the corresponding switches.

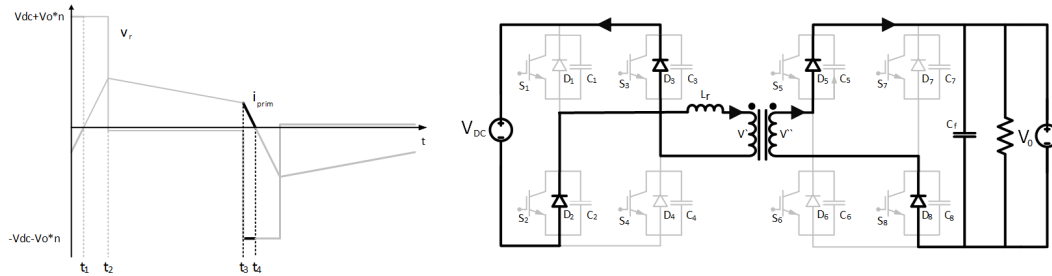


Fig. 4.16 DAB. Freewheeling interval $t_3 < t < t_4$

$t_3 < t < t_4$ • Now, the maximum negative voltage is applied across V_r it is the time for S_2 and S_3 to conduct. However, it is not possible, because the main current flows in the reverse direction and the IGBTs conduct only in one direction. The current dies out through the diodes D_2, D_3, D_5 and D_8 at a rate equal to

$$\frac{\partial i_3}{\partial t} = \frac{-V_{DC} - V_o/n}{L} \quad (4.28)$$

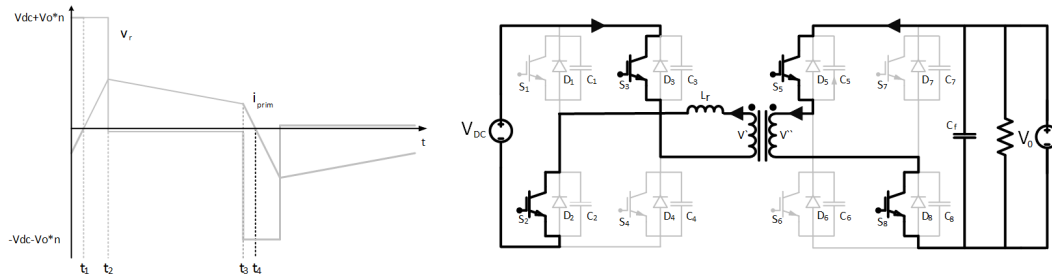


Fig. 4.17 DAB. A current reverse $t = t_4$

$t = t_4$ • At this instant, the main current reverses. D_2, D_3, D_5 and D_8 become reverse biased and the negative current continues to flow through the switches S_2, S_3, S_5 and S_8 which now become forward biased. The voltage across the switches equals to zero, due to previously recharged capacitors. The effect is turn-off of the freewheeling diodes without reverse recovery losses and lossless turn-on of the corresponding IGBTs.

According to [9], the output power of the converter is equal to

$$P = V_{DC} I_L = \frac{V_{DC} V_o/n}{\omega L} \phi \left(1 - \frac{\phi}{\pi}\right) \quad (4.29)$$

The converter will not transfer any power if the angle ϕ is set to 0 and at $\pi/2$ the maximum power transfer is reached. A general expression for finding required inductance is:

$$L = \frac{V_{DC} V_o/n}{\omega_L P} \phi \left(1 - \frac{\phi}{\pi}\right) \quad (4.30)$$

In this thesis, phase shift angle $\phi = \pi/4$ was chosen for solving the equation. Two different inductances were calculated for two operating frequencies.

Table 4.1: Calculated leakage inductances for the DAB topology. P=2.7 MW

Frequency	2000 Hz	10000 Hz
L_{leak}	225 μH	45 μH

4.4 Transformer design

The transformer is the bulkiest part of the converter. It is a massive high-voltage construction which consists of copper windings, insulation and a soft-magnetic core which is the heaviest part of the transformer. The core main duty is to enhance the magnetic field produced in the primary winding and to forward it to the secondary winding. There are two main types of losses in any transformer. They are copper losses which are incurred by the resistivity of copper windings and core losses. The core losses in turn are subdivided into hysteresis losses and eddy current losses.

It is hard to reduce the copper losses. The diameter of the wire is defined by the operational current and the thickness of the wire should be sufficient enough to prevent overheating of the winding. It is not possible to reduce the length of the wire in a winding as well, because the transformer requires specified number of turns of specified perimeter to achieve desired operational point. The length of the wires used for primary and secondary windings are

$$l_{wire_1} = N_1 l_p \quad (4.31)$$

$$l_{wire_2} = N_2 l_p \quad (4.32)$$

where N_1 and N_2 are the number of turns of the primary and secondary winding respectively and l_p is the perimeter of one loop. Knowing the length and the diameter of a wire it is possible to find its resistance

$$R_1 = \rho_{cu} \frac{l_{wire_1}}{\phi_{wire_1}} \quad (4.33)$$

$$R_2 = \rho_{cu} \frac{l_{wire_2}}{\phi_{wire_2}} \quad (4.34)$$

ρ_{cu} the resistivity of copper and is equal to $1.68 * 10^{-8} \Omega m$. Now, the total copper losses can be calculated as

$$P_{cu} = R_1 I_1^2 + R_2 I_2^2 \quad (4.35)$$

The core losses strongly depend on a material and that is chosen for the transformer core. There are a lot of various magnetic materials and structures that are used in industry nowadays. They differ by price, losses per unit, recommended operational frequency, magnetic properties, density etc. Core losses are subdivided into two groups: hysteresis losses and eddy current losses.

- Atomic dipoles in magnetic materials align with the applied magnetic field. When the field is removed, part of them may return to the previous position, one part stays aligned in the same direction and the rest take some other position. Now, if the field is applied in the opposite direction some of energy need to be spent to reverse and align all those dipoles in the new direction. This phenomenon is called hysteresis loss. The more dipoles that stay aligned after the field disappears, the larger the losses are. Soft-magnetic materials are usually characterised by a formula

$$P_{hy,loss} = k f^\alpha \hat{B}^d \quad (4.36)$$

where f is operating frequency, \hat{B} is peak flux density, k , α and d are specific coefficients for a particular material.

- Eddy current loss is the loss caused by parasitic currents induced around a closed magnetic loop in a thick piece of conductive material. A magnetic core is often a very massive object depending on the power rating of an application. Extremely large eddy currents would have been induced in this magnetic loop if it would have been made solid. To overcome this problem, the magnetic loops are divided into thin laminations electrically isolated between each other. The thinner a lamination is, the lower the eddy current losses are, due to the reduced path for the induced currents. Another tactic is the utilization of powder materials which are described below.

There are three main groups of magnetic cores used in the industry nowadays:

- Ferrite cores has been known for a long time. Ferrites are ceramic materials which mostly consist of iron oxide with such additives as oxides or carbonates of manganese and zinc or nickel and zinc. Ferrite cores are very popular in switched-mode power supplies and used in applications with frequencies up to 1-2 MHz. Such materials have a narrow hysteresis loop. Consequently, they will not store much energy and in case of t.ex. flyback converter or inductor a gap must be added. [10]
- Metal Alloy Tape-Wound Cores are suitable in low-frequency applications. The main material used in such cores is Permalloy - a nickel-iron alloy which has almost ideal characteristics at low-frequencies with an extremely high permeability $\mu = 60000$, a high saturation flux density $B_{max} = 0.9T$ and a narrow hysteresis loop. Unfortunately, the material structure is very suitable for the initiation of eddy currents. That is why the Permalloy cores are built of thin tape-wound laminations. However, even extremely thin laminations do not help to get rid of eddy current at high frequencies. Instead, amorphous metal alloys are used in applications up to 100-200 kHz. In this thesis, VITROPERM 500 is used for the transformer cores due to its extremely low losses. Fig. 4.18 shows a comparison of different tape-wound cores. [10]

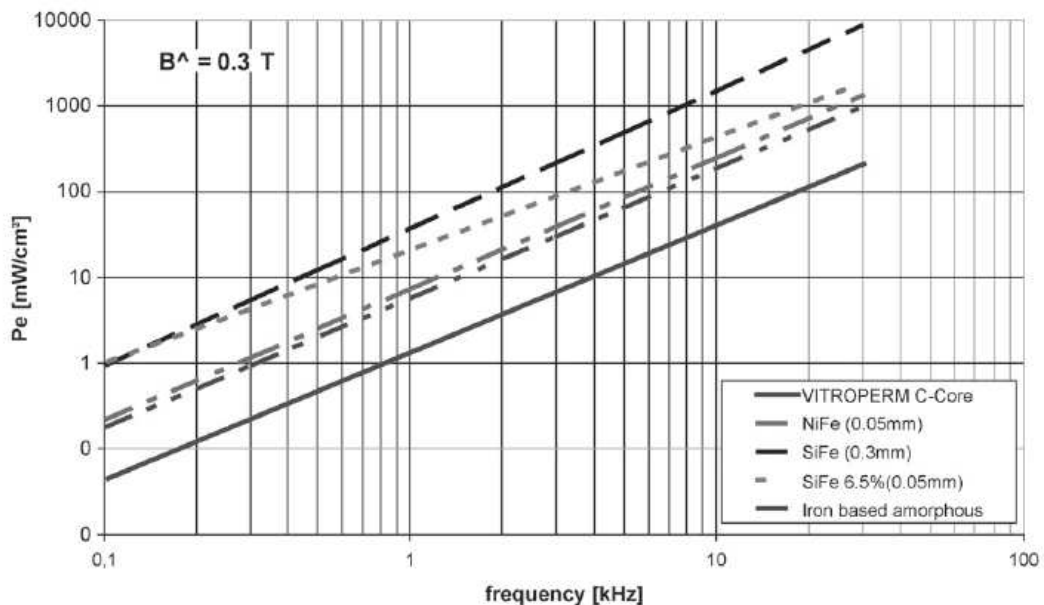


Fig. 4.18 Losses vs frequency of cores made of different materials with closed airgap. [1]

The material has a high saturation flux density $B_{max} = 1.2T$ and a high permeability $\mu = 20000 \dots 50000$. One tape thickness is approximately $18 \mu m$.

- Powdered Metal Cores are composite materials with a distributed air gap throughout the entire core. Such a core consists of small soft-magnetic particles isolated between each other by a non-magnetic material. They have a relatively low permeability and a high magnetizing current. Such cores are very

suitable for the DC inductor applications and is used for the output filter design in this thesis and not so good for switched-mode power supply transformers. [10]

When the magnetic material is chosen, a core shape should be chosen. In this thesis, a double-E core is used due to its simplicity. In Fig. 4.19 optimum dimensions for the core and a coil former are depicted, where $b_a = a$, $d = 1,5a$, $h_a = 2,5a$, $b_w = 0,7a$ and $h_w = 2a$.

The transformer power rating strongly depends on the amount of magnetic material. The main equation for the transformer calculation is

$$S = V_{pri} I_{pri} = 2k_{cu} f A_{core} A_{window} J_{rms} \hat{B} \quad (4.37)$$

where, S is the volt-ampere rating of the transformer, V_{pri} is the input voltage and in this particular case it is equal to V_{DC} , I_{pri} is the input current, k_{cu} is a filling factor which defines how much winding is allowed inside the core window, f is the operating frequency, A_{core} is the cross-sectional area of the core leg, A_{window} is the area of a window inside the core, J_{rms} is maximum allowed current density in the windings and \hat{B} is the allowed flux density inside the core.

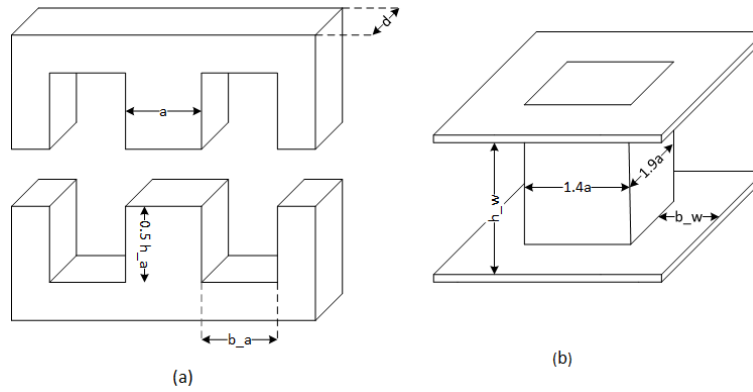


Fig. 4.19 (a) a double-E core (b) core former

From Fig. 4.19 it is seen that:

$$A_{core} = ad = 1,5a^2 \quad (4.38)$$

$$A_{window} = h_a b_a = 1,4a^2 \quad (4.39)$$

$$A_{core} A_{window} = 2,1a^4 \quad (4.40)$$

The multiplication of these two areas is called area-product and this is an important parameter which characterises power rating of the transformer. By inserting (4.40) into (4.37), the parameter a can be calculated as

$$a = \sqrt[4]{\frac{S}{4.662k_{cu} f J_{rms} \hat{B}}} \quad (4.41)$$

The filling factor for a high-voltage application is usually chosen to be between 0.05...0.2. In this thesis, the output voltage is $V_o = 40000V$ and $k_{cu} = 0.2$. The suitable current density is $J_{rms} = 1.5A/m^2$. Some part of the magnetic flux produced in the magnetic circuit does not link the windings. This flux results in leakage inductance which is utilised in resonant topologies as a part of resonant tank, however in conventional hard-switched topologies it is undesired or considered as a parasitic element. Leakage inductance of the transformer can be adjusted by alternating layers of the windings and modifying the thickness of insulation between those layers. A general expression is:

$$L_{leak} \approx \frac{\mu_o N_{pri}^2 l_w}{p^2 h_w} \left(\frac{b_{cu}}{3} + b_i \right) \quad (4.42)$$

Table 4.2: Calculated dimensions of double E-core

	SAB		DAB	
frequency	2000 Hz	10000 Hz	2000 Hz	10000 Hz
n	0.08	0.08	0.09	0.09
\hat{B}	0.45 T	0.45 T	0.25 T	0.18 T
L_{leak}	48.19 μH	5.66 μH	222 μH	44.81 μH
A_{window}	0.068 m^2	0.029 m^2	0.058 m^2	0.0355 m^2
A_{core}	0.073 m^2	0.012 m^2	0.062 m^2	0.0381 m^2
core width	0.88 m	0.576 m	0.81 m	0.637 m
core height	0.7532 m	0.5037 m	0.71 m	0.5574 m
core length	0.33 m	0.22 m	0.31 m	0.24 m
core volume	0.15 m^3	0.04 m^3	0.11 m^3	0.0545 m^3
core weight	1067 kg	295 kg	834 kg	399 kg

where $l_w \approx 9a$ is mean turn length, b_i is the insulation thickness between adjacent layers of the windings, b_{cu} is the total width of the copper in the winding window, p is the number of interfaces between winding sections.

When it comes to the determination of the number of turns, the window area designed for the windings may be assumed equally divided between the windings.

$$\frac{A_w}{2} = A_{pri} = A_{sec} = \frac{N_1 A_{cu,pri}}{k_{cu}} = \frac{N_2 A_{cu,sec}}{k_{cu}} \quad (4.43)$$

where $A_{cu,pri}$ and $A_{cu,sec}$ are the total copper areas of the primary and secondary windings respectively. Now, the number of turns are given by:

$$N_1 = \frac{A_w * k_{cu}}{A_{wire1} + A_{wire2}/n} \quad (4.44)$$

And

$$N_2 = \frac{N_1}{n} \quad (4.45)$$

Another thing is that the ratio of the transformer used in the phase-shifted converter should be somewhat lower than if it would be used in a conventional converter.

In this thesis, the eddy current losses are neglected because the structure of the chosen core material minimises this phenomenon. However, hysteresis losses are significant and need to be included in the analysis. As it comes from (4.36), these losses depend on the frequency f and the magnetic flux density \hat{B} . The operational frequency of the studied converters is fixed. However, the flux density changes if the input voltage across the primary winding decreases. In general, Faraday's law implies;

$$e(t) = v_{prim}(t) = N \frac{d\phi}{dt} = N A_m \frac{dB}{dt} \quad (4.46)$$

In case of a square-wave supply, the voltage across the primary winding takes three different values: V_{DC} , $-V_{DC}$ and 0. Hence, maximum flux density corresponds to peak voltage across the winding. Since an inverter produces square-waved voltage across the primary winding, integration of the function gives

$$V_{prim} = \int_0^{DT} V_{DC} dt = V_{DC} DT = \frac{V_{DC} D}{f} \quad (4.47)$$

Integration of (4.46) substituted in (4.47) gives

$$\hat{B} = \frac{V_{DC} D}{4 A_m f N_{prim}} \quad (4.48)$$

Now, (4.36) can be used and loss per volume unit can be easily calculated. To acquire total hysteresis loss in the core the result need to be multiplied with the total volume of the yoke.

4.5 Resonant components

In this thesis, no additional resonant components were added to achieve soft-switching. Only parasitic elements, such as output capacitances of IGBTs and transformer leakage inductance were utilised.

4.6 Output filter design

The output filter is an essential component of any power converter. It increases the quality of the output by reducing voltage and current ripples produced during the conversion. In another words, the output filter specifies the limits of the output voltage and current. In this thesis, the desired output limits are

$$\Delta V = 0.01V_o \quad (4.49)$$

$$\Delta I = 0.1I_o \quad (4.50)$$

which means that the output voltage can vary between $\pm 0.5\%$ and the limit for the current variations is $\pm 5\%$ of the average value. There are two main components used in a design of the passive output filter and each of them carries its special function. The first one is an inductor placed in series with the load which suppresses the voltage ripple and a parallel capacitor with a property to provide smooth output current.

4.6.1 Output inductor

The output inductor performs as a filter when the incoming voltage fluctuates or changes. There are two main parts in any inductor. The first one is the winding and its ability is to create a magnetic field. It consists of one or several loops of a conductive wire which form a coil and if a voltage is applied to the both ends of the wire, the electrical current will maintain the electromagnetic field inside and around the winding. The second component is the magnetic core which is situated inside the winding. It consists of a soft-magnetic material and its ability is to enhance the produced electromagnetic field by increasing the flux inside it. Hence, dimensions of the inductor decrease. Any change in the voltage would influence the produced electromagnetic field which affects the flux cutting every loop of the winding. In response, the flux creates the voltage in all the turns that is opposite to the changed voltage.

Any inductor is characterised by the inductance it can produces. The voltage across an inductor is given by

$$v_L = L \frac{di_L}{dt} \quad (4.51)$$

where di_L is the ripple of the current which flows through this inductor and dt is a time when the voltage is applied. As it is seen from the full-bridge topology, the voltage across the inductor is a difference between rectifier and converter output voltages

$$v_L = V_{rectifier,out} - V_o = \frac{N_2}{N_1} V_{DC} - V_o \quad 0 < t < t_{on} \quad (4.52)$$

By combining the two previous equations, the necessary filter inductance is given by

$$L_f = \frac{(nV_{DC} - V_o) D_{eff}}{\Delta I_o \cdot 2f} \quad (4.53)$$

where D_{eff} is the duty cycle of the output voltage, ΔI_o is the desired current ripple and $2f$ is the frequency of current oscillations which is doubled compared with the converter operating frequency. The designing process can be started with a calculation of the wire thickness. Generally, in another words, the current density should be specified within some limits considering operating temperature. Typical current density values used in power electronics are between $J_{max} = 4.6A/mm^2$. Bearing that in mind and knowing that the area of round conductor is equal:

$$A_{conductor} = \frac{\pi}{4} d_{conductor}^2 \quad (4.54)$$

$$\frac{I_{rms}}{A_{conductor}} \leq J_{max} \quad (4.55)$$

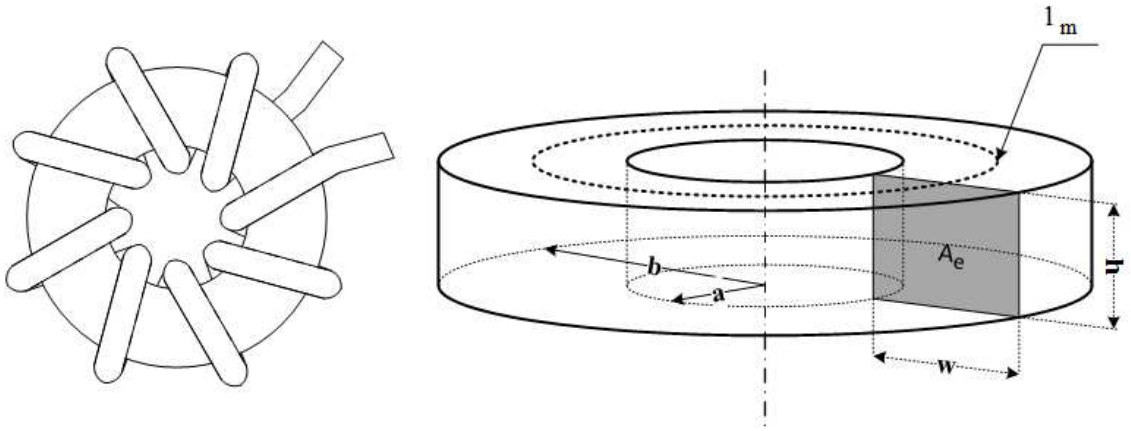


Fig. 4.20 Toroidal inductor

the diameter of the conductor can be obtained from

$$d_{conductor} \geq \sqrt{\frac{4I_{rms}}{\pi J_{max}}} \quad (4.56)$$

This value is not the final diameter of the wire since insulation around the conductor should be added. 2-4 mm of insulation is enough between two adjacent loops of the winding. A thick layer of insulation fully covers the core as well. There are many different types of inductor cores which differ by size, shape and materials used. In this thesis, the inductance is rather large and the current is relatively high. It means, that the core of the filter acquires large dimensions which leads to a high volume of magnetic material. The toroidal form of the core was chosen for this application because they are the cheapest on the market with respect to the volume and the production cost. In Fig.4.20 a schematic drawing of a toroid with rectangular cross-section A_e is depicted. Here, a is the inner diameter, b is the outer diameter, h is the height and l_m is the length of the magnetic path. According to [13], it is necessary to take into account the insulation in the calculations because all the turns should fit on the toroid. Consequently, a constraint can be defined as

$$2(a - d_{conductor})\sin\frac{\theta}{2N} > d_{conductor} \quad (4.57)$$

where θ is an angle between two adjacent loops of wire and N is a number of turns on the toroid. According to Amperes law, the current i passing through a winding with N turns and the mean length l_m will cause a field intensity of:

$$H_m = \frac{Ni}{l_m} \quad (4.58)$$

In case of a toroid with square cross-section the field is not uniform inside:

$$B_o(r) = \frac{\mu_o NI}{2 * \pi r} \quad (4.59)$$

The flux through each turn is:

$$\Psi = \iint \vec{B} * d\vec{s} = \frac{h\mu_o NI}{2\pi} \int_a^b \frac{dr}{r} = \frac{\mu_o NI h}{2\pi} \ln \frac{b}{a} \quad (4.60)$$

It is given that $b/a > 1$. A good approximation is

$$\ln \frac{b}{a} \approx 2 \frac{(b-a)}{(b+a)} \quad (4.61)$$

Now, the inductance can be written as

$$L = \frac{\mu N^2 h (b-a)}{2\pi \left(\frac{b+a}{2}\right)} = \mu_o N^2 \frac{A}{l_m} \quad (4.62)$$

Table 4.3: Output inductor calculated data

frequency	2000 Hz	10000 Hz
inductance L_f	83 mH	17 mH
\varnothing_{in}	0.26 m	0.15 m
\varnothing_{out}	0.55 m	0.31 m
core weight	293 kg	61 kg

According to the [13], height-width ratio $\frac{h}{w} = 2$ and inner-outer radii ratio equal to $\frac{a}{b} = 0.5$ provide minimal core losses.

The approximated length of the magnetic conductor is equal to a circumference which radius is equal to the arithmetical mean of inner and outer radii.

$$l_m = 2\pi \frac{b+a}{2} = 4\pi a \quad (4.63)$$

Now, by choosing an appropriate magnetic field strength H_m inside a loop in accordance with selected material and by combining (4.58), (4.62) and (4.63) the dimensions of the core can be calculated. The results are shown in Table. 4.3.

4.6.2 Output capacitor

The purpose of the output capacitor is to take over current ripples that passes through the output inductor and to deliver a smooth DC-current for the output. In this case, the ripply inductor current can be denoted as a sum:

$$i_L = i_C + I_o \quad (4.64)$$

The average inductor current is equal to the DC-output current $I_L = I_o$. Hence, the capacitor current can be expressed as

$$i_c = i_L + I_L \quad (4.65)$$

where i_c is a linear function, shown on Fig. 4.21a. The instant voltage across the capacitor is given by:

$$v_c(t) = v_c(t_o) + \frac{1}{C} \int_{t_o}^{t_o+T_s} i_c(t) dt \quad (4.66)$$

The equation implies that the capacitor voltage at time t is equal to the voltage at time t_o plus the integral of the capacitor current in given period of time. The output voltage ripple is depicted in Fig. 4.21b. It is

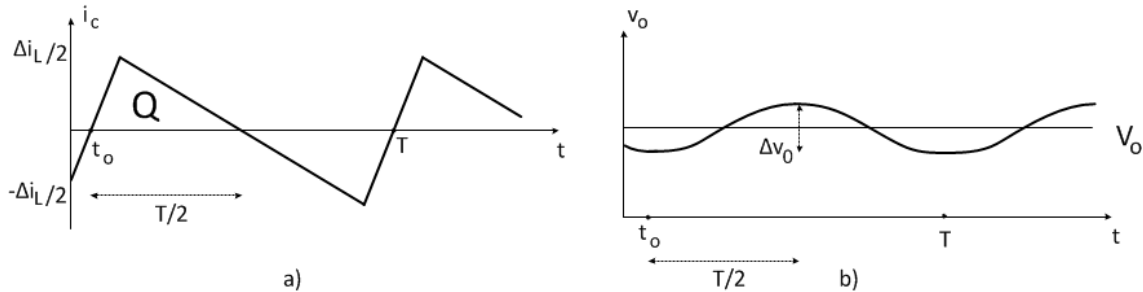


Fig. 4.21 (a) capacitor current (b) output voltage ripple

seen, that the current ripple is positive for the first half of the cycle from t_o to $t_o + \frac{T_s}{2}$. During this time, the capacitor voltage changes from its minimum value to the maximum peak value which is actually the peak-to-peak output voltage ripple:

$$\Delta v_o = v_c(t_o + \frac{T_s}{2}) - v_c(t_o) = \frac{1}{C} \int_{t_o}^{t_o+T_s/2} i_c(t) dt = \frac{Q}{C} \quad (4.67)$$

The integral of the capacitor current equals the charge Q put into the capacitor. It can be easily calculated if the geometry of the waveform is known. As it is seen from Fig. 4.21a, the charge in this particular case equals to the triangular area. The required capacitance can be calculated by

$$C = \frac{Q}{\Delta v_c} = \frac{1}{2} \frac{\Delta i_L T_s}{2} \frac{1}{2} \frac{1}{\Delta v_c} = \frac{\Delta i_L}{8f\Delta v_c} \quad (4.68)$$

Δi_L and Δv_c are the required parameters of the output filter which are defined in the beginning of this section. The capacitances used in this thesis are the same for the both topologies. However, converters with a higher operational frequency require less inductance. The calculated results are shown in Table. 4.4:

Table 4.4: Output capacitor calculated data

frequency	2000 Hz	10000 Hz
capacitance	527 nF	105 nF

Chapter 5

Simulation verification

5.1 Simulation of Single active bridge (2, 10 kHz)

In this section two configurations of the SAB full-bridge converter are investigated. Both of the models are simulated using MATLAB Simulink. The project diagram is shown in Fig. 5.2. The blocks used for the simulations are the same for both configurations. However, the parameters of the components are changed in accordance with the operational frequency. The settings for the semiconductor blocks are taken from the actual datasheets that was mentioned before. The IGBTs are defined by the on-state resistance R_{on} , the forward voltage drop V_f and the current fall time t_{fi} . The capacitance of the switches is set to zero. Instead, capacitive snubbers are placed across the switches. The settings for the power diodes are the on-state resistance R_{on} , the forward voltage drop V_f and no snubbers. The resistances of the windings are included. The tailing currents which are typical for the IGBT transistors are set to zero due to the absence of such parameter in the used datasheets. Most likely, this parameter is already included in the current fall time t_{fi} . The transformer magnetising resistance and inductance are set equal to $500 pu$.

The switching waveforms of the 2 kHz converter are shown in Fig. 5.1. The two left figures represent the

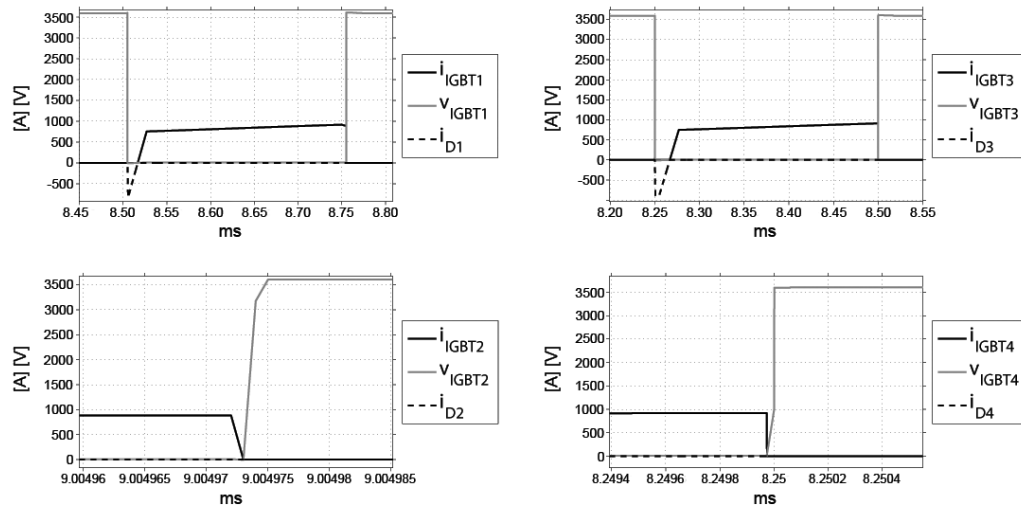


Fig. 5.1 SAB. IGBT voltage and current waveforms. $f = 2kHz$

leading leg and the two right figures show the behaviour of the lagging leg. The waveforms of the transistors sitting on the same leg are identical but are shifted half a cycle in accordance with each other. The upper pictures, which show an overview of one typical conduction period, give an explanation of how the legs got their names. The black solid line shows the current which passes through the transistors. As it is seen from the figures, the current through the left switch starts to rise somewhat earlier than in the case of the right switch. Hence, the leading transistor carries more current than the lagging one and its conduction time is longer. Subsequently, the leading freewheeling diodes are less loaded than the lagging ones. The diode cur-

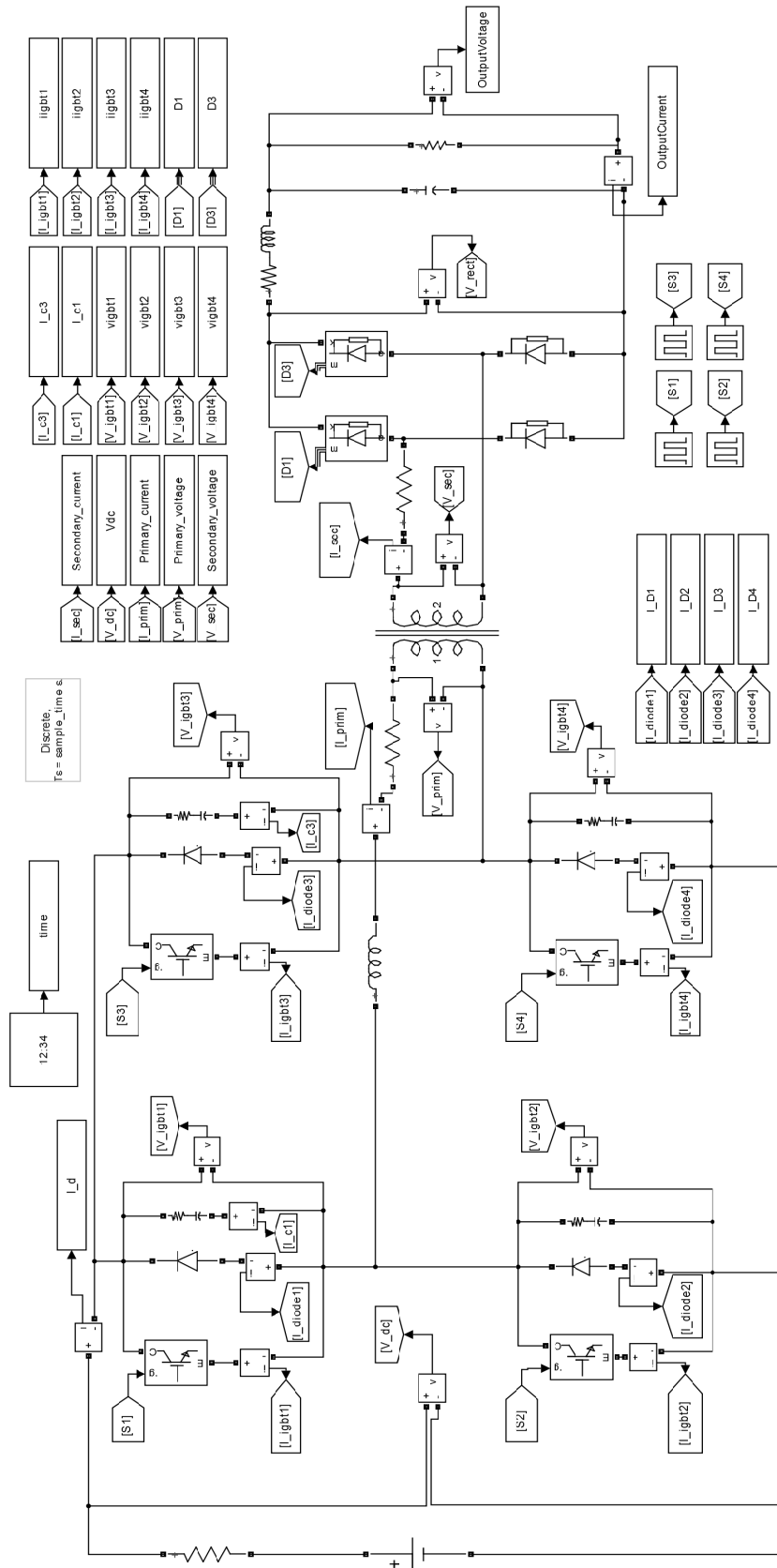


Fig. 5.2 MATLAB simulation model of Single active bridge topology

rent is shown with the grey dashed line. The grey solid line shows the voltage across the transistors.

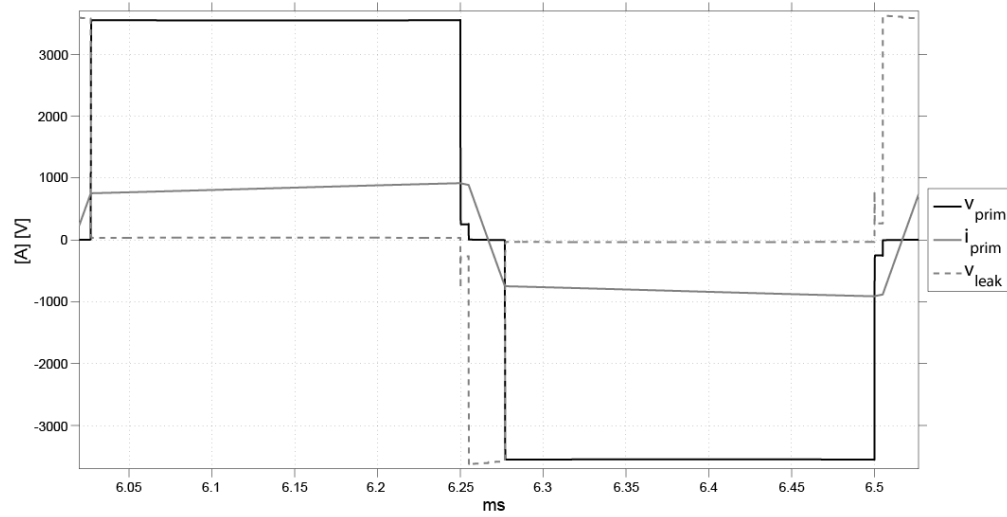


Fig. 5.3 SAB. Transformer and leakage inductance waveforms $f = 2kHz$

It is seen from the lower figures, that the transistors turn off without any losses because the current drops before the voltages increase. So, the multiplication of these two curves equals zero. The situation with the turn-ons is similar. It is seen on the upper pictures, that before and after the instant when the freewheeling diode current transfers into the switches, there is no applied voltage across the corresponding devices. That means there is no reverse recovery losses and the switches turn-on without any losses.

According to the described waveforms, it is possible to claim that in case of the SAB topology, only conductive losses are inherent for the semiconductors, situated on the primary side. When it comes to the secondary side, the reverse recovery losses are unavoidable and both conductive and switching losses should be considered.

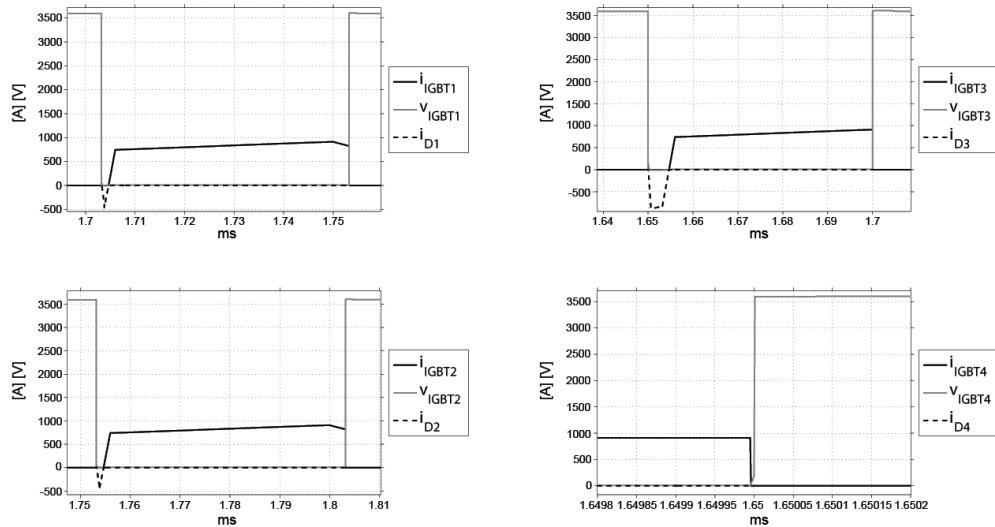


Fig. 5.4 SAB. IGBT current and voltage waveforms $f=10kHz$

Fig. 5.3 shows the voltage and the current across the primary winding of the transformer. When the full voltage V_{DC} is maintained across the winding, the main current rises linearly. This interval is referred to the power transfer interval when the two diagonal switches are closed. In this case a very small positive voltage is maintained across the leakage inductance. At $t = 6.25ms$ one of the switches turns off and the first transient occurs. In theory, the voltage across the primary winding should become equal to zero. This does not occur in the simulation due to some energy stored in the leakage inductance. The voltage across the leakage inductance is indicated with the grey dashed line. After the first transition, the clamped freewheeling interval occurs. During this time, the main current linearly decreases as it should according to the theory until the second transition occurs and the voltage across the leakage inductance obtains a very high negative value. This voltage forces the main current to decrease very fast. It is also seen, that there is a very small voltage across the primary and, hence, the secondary winding. During this time all the four rectifier diodes conduct. At the end of the freewheeling interval the main current reverses and continues to flow through the switches at the same rate. When the secondary side is no longer short-circuited, the voltage across the leakage inductance becomes slightly negative and a new power transfer period begins.

Fig. 5.4 shows the results of the 10 kHz simulation. The behaviour is typical for the ZVS full-bridge converter. The sequence of the events starts from the fourth picture and continues counter-clockwise. At 1.65 ms $IGBT_4$ stops to conduct current and a lossless turn-off occurs. Directly after that, the recharge of the capacitors C_3 and C_4 takes place. This event can be verified by the instant change of the voltage levels across those capacitors and, hence, the transistors. The voltage across $IGBT_4$ increases to V_{DC} while the voltage across $IGBT_3$ drops to zero. After this transition, the main current continues to freewheel through the diode D_3 . When this current dies out a lossless turn-on of $IGBT_3$ occurs. The switch continues to conduct until 1.7 ms when another transition takes place accompanied with a lossless turn-off of the transistor. Now, the capacitors C_1 and C_2 accomplish the recharge and the voltage across $IGBT_1$ is removed. Subsequently, the main current flows through D_1 and then $IGBT_1$ turns on without any losses at $t = 1.7045ms$. The lossless turn-off of the device occurs at $t = 1.7532ms$. The description stops here, because the picture that represents the $IGBT_2$ waveforms shows only the turn-off of the device, just to verify that both of the legs have no switching losses.

The transformer primary voltage and current waveforms, which are shown in Fig. 5.5, are similar for both of the operating frequencies.

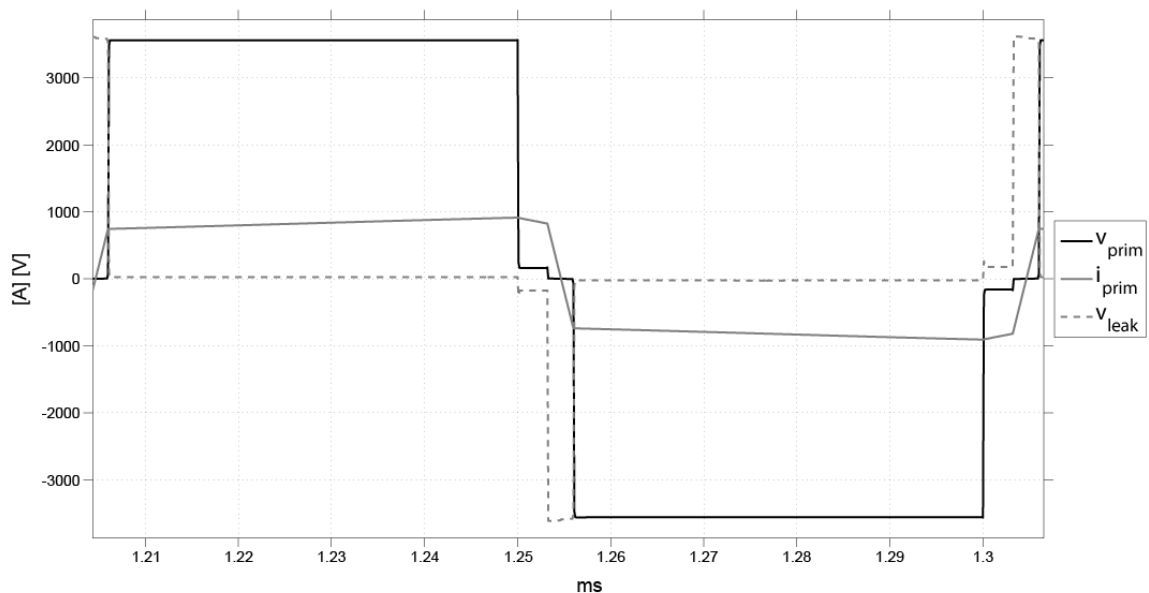


Fig. 5.5 SAB. Transformer and leakage inductance waveforms $f=10\text{ kHz}$

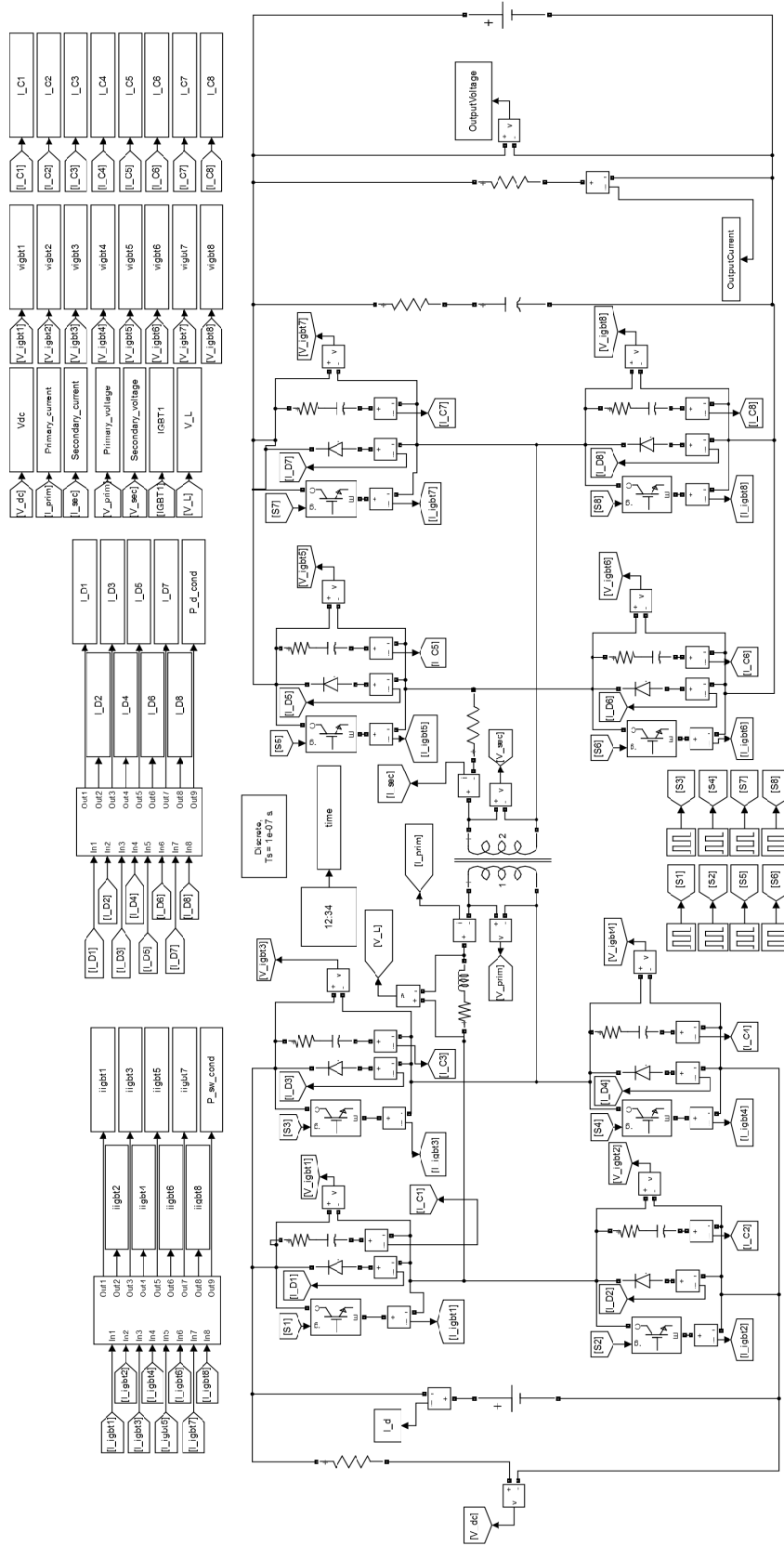


Fig. 5.6 DAB Simulink project diagram

5.2 Simulation of Dual active bridge (2, 10 kHz)

In this section, the results from the simulations of the Dual active bridge dc/dc converter are presented. The project diagram used in Simulink is shown in Fig. 5.6. The block settings are similar to the previous case. In the simulations two voltage sources are used. One on the primary side, and another is placed across the load. Two voltage sources are necessary for the proper functioning of the Dual active bridge converter. As a matter of fact, this action does not conflict with the realistic operational conditions of the converter. In reality, the secondary voltage source appears to be the grid or an HVDC line where the voltage level is fixed.

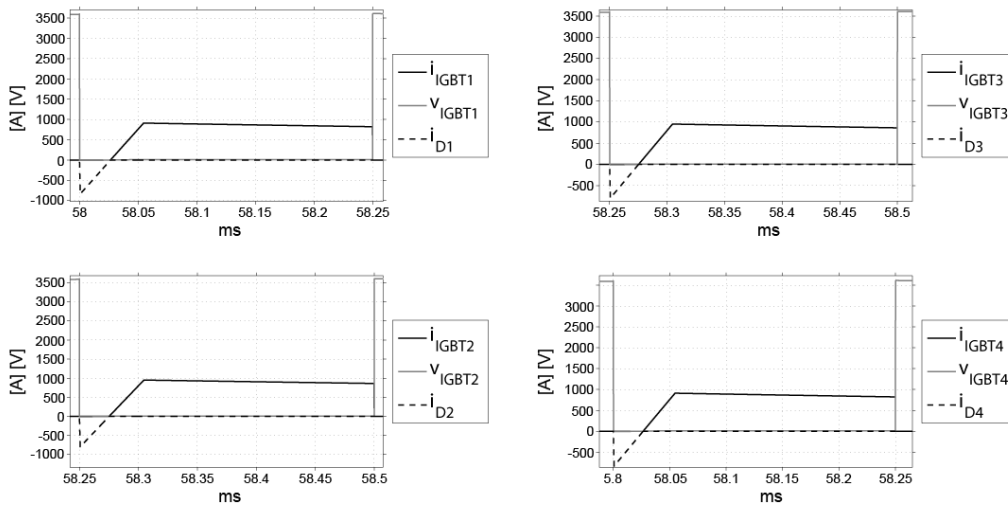


Fig. 5.7 DAB. Low voltage side waveforms. 2000 Hz

Again, in the beginning, results from the 2000 Hz simulation are presented. In Fig. 5.7 the primary side transistor waveforms are shown. The secondary side waveforms are depicted in Fig. 5.8. The voltages across the secondary switches are decreased 100 times on the plots, otherwise the currents would not be seen on the figures.

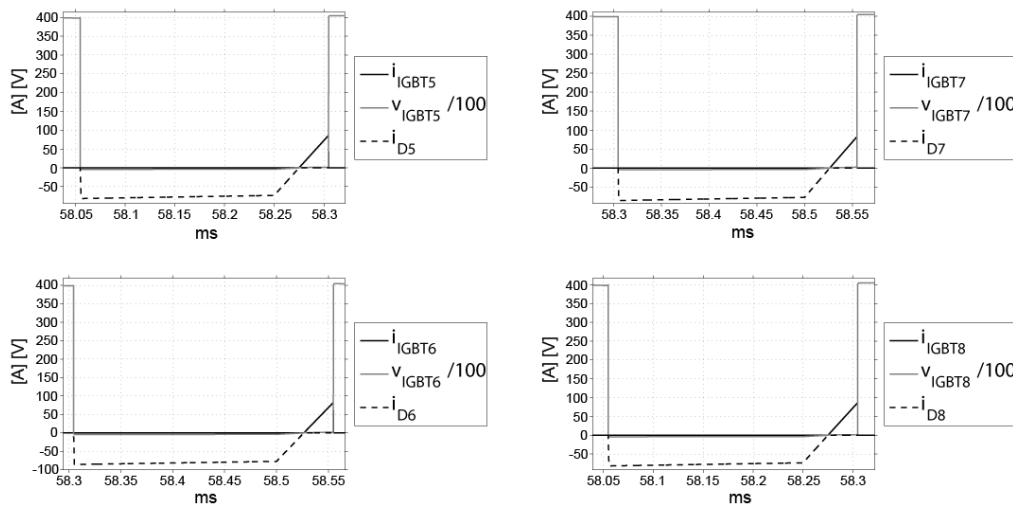


Fig. 5.8 DAB. High voltage side waveforms. 2000 Hz

It is seen, that the primary switches conduct more current than the primary diodes, while the secondary diodes dominate on the high voltage side and the secondary S_5 , S_6 , S_7 and S_8 conduct only very little

current.

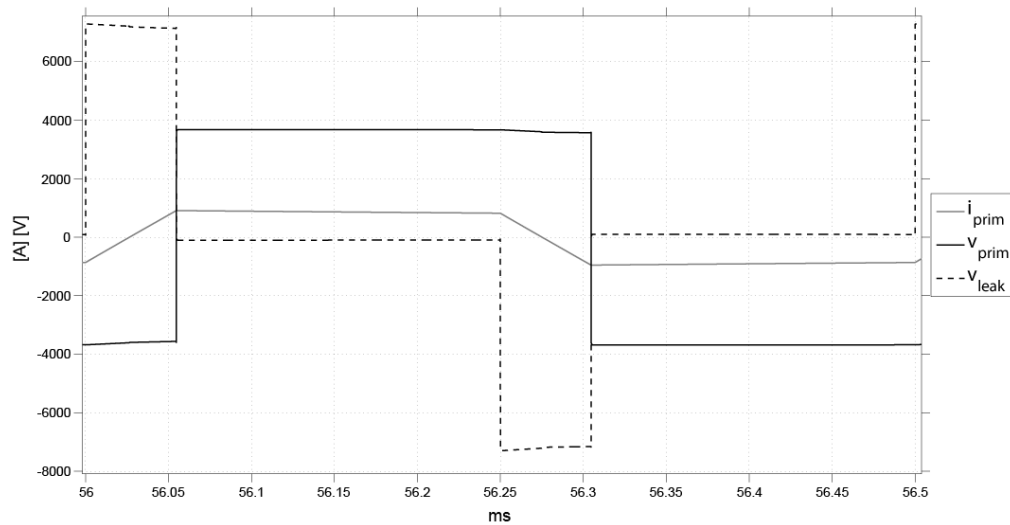


Fig. 5.9 DAB. Transformer and leakage inductance waveforms. 2000 Hz

The main advantage of this converter is that the switching and the reverse recovery losses are not present. Every conduction interval starts with the current through a freewheeling diode. The diode current slowly drops to zero and no reverse recovery losses occur because the voltage across the diode and, hence, the transistors is still zero. Then, the current reverses and turns on the switch without a switching loss. When it is time for a transistor to switch-off the current goes in to the parallel capacitor which delays the voltage step and allows the IGBT to turn off losslessly.

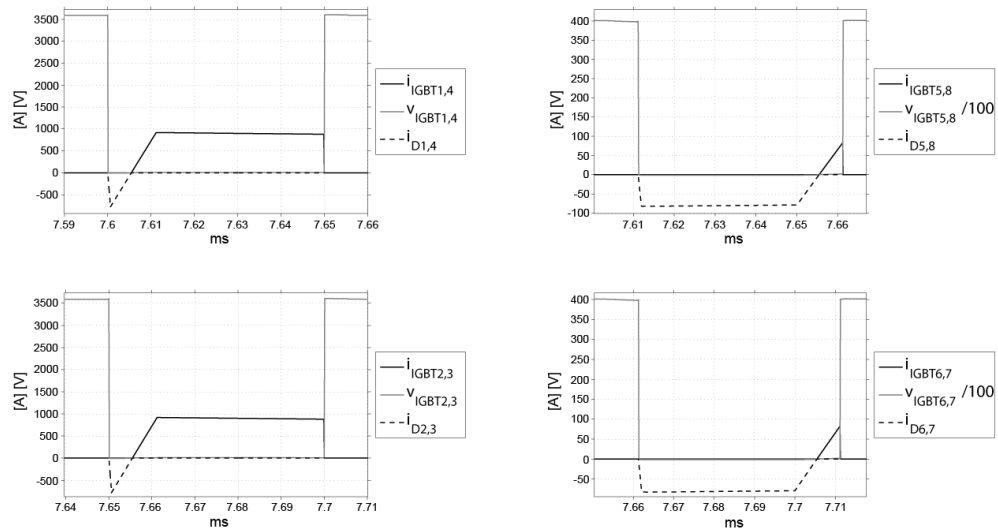


Fig. 5.10 DAB waveforms. 10000 Hz

In Fig. 5.10 the waveforms from the 10000 Hz simulation are shown. One picture represents one of the four diagonal pairs of the switches. The waveforms look very similar to the case with 2000 Hz, but with shorter period. It is seen that the diodes turn off without the reverse recovery losses and the switches turn on without any stress at all.

Lossless turn-off of the active components is shown in Fig. 5.11. One picture represents a diagonal pair of the switches. It is clearly seen, that the current in all the switches drops before the voltage rises. Hence,

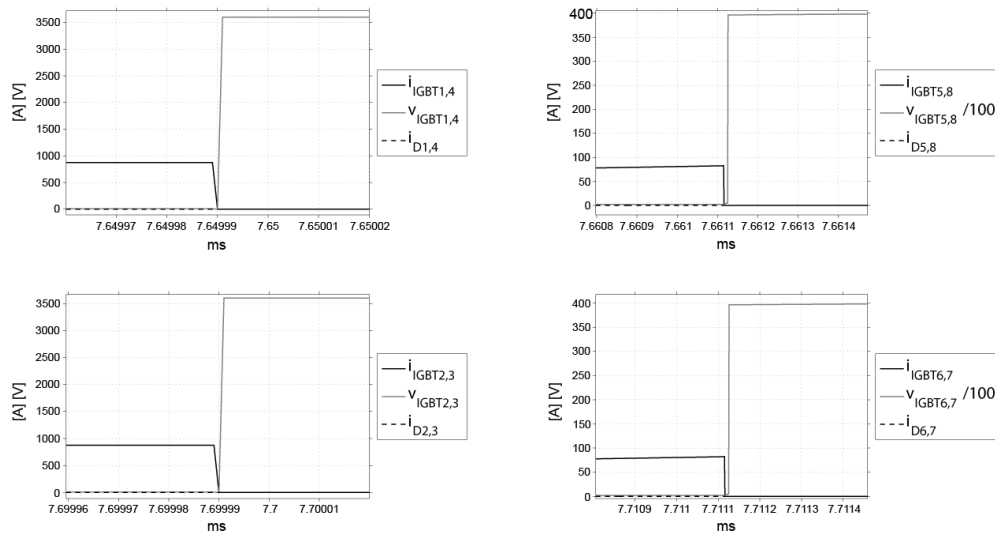


Fig. 5.11 DAB. Lossless turn-offs of the switches. 10000 Hz

multiplication of these curves at the turn-off gives zero losses.

From the obtained waveforms, it is seen that only conductive losses are present in this operational mode. No reverse recovery losses in the diodes or switching losses in the transistors were observed.

5.3 Calculation of losses

In this section, the losses of the simulated converters are presented. The following components are taken into account: the IGBTs, the freewheeling diodes and the rectifier diodes, the magnetic cores and the windings. In case of the transistors, only conduction losses were calculated due to provided lossless on and off transitions of the IGBTs. In case of the diodes, both conduction and reverse recovery losses were calculated. Both types of the losses are typical for the diodes situated in the rectifying stage of the SAB topology. However, the reverse recovery losses in the freewheeling diodes are neglected. The reason for this is that after every conduction time, the diode current is being redirected into a parallel IGBT. This means that the voltage across the diode becomes equal to the forward voltage drop of the transistor which is very low and cannot cause noticeable reverse recovery loss.

The average values of R_{on} and V_f were used for the semiconductor blocks, since they do not support a dynamic change of these settings. For the precision, new values were calculated and updated into the blocks after every simulation in accordance with the previously obtained currents. Lookup tables were implemented in Simulink for obtaining the forward voltage drop curves. To find the conduction losses in a semiconductor, the integral of the voltage drop function was multiplied with the integral of the current function.

The losses in the transformer core and the inductor core were obtained from the datasheets in accordance with the operating frequency and calculated volume of the elements. No eddy current losses were taken into account.

The results from the calculations of the losses are presented in Table. 5.1. It is seen that the DAB topology outperforms the Single active bridge concerning energy efficiency. The reason is the absence of the reverse recovery losses which make up the largest portion of the total losses in case of the SAB topology. The inductor losses are also not present in the DAB converters due to the absence of such element in the topology.

Table 5.1: Calculated losses

Frequency	SAB		DAB	
	2000 Hz	10000 Hz	2000 Hz	10000 Hz
Inductor core losses	125 W	27 W		
Inductor winding losses	429 W	155 W		
Rectifier diode rr losses	10403 W	52013 W		
Transformer core losses	1702 W	9059 W	413 W	1336 W
Transformer winding losses	505 W	160 W	903 W	722 W
IGBT conduction losses	6353 W	6370 W	6885 W	6460 W
Diode conduction losses	6402 W	6417 W	5258 W	6777 W
Total losses	25919 W	74201 W	13459 W	15295 W
Efficiency	99.04 %	97.25 %	99.50 %	99.43%

5.4 Lossless range

All of the four converters were simulated at a different power supply levels. In case of the SAB converters, the conduction time of the leading diodes shows if the converter is still in the lossless region. When there is no current through the diodes D_1 and D_2 , it means that the current through the corresponding switches $IGBT_1$ and $IGBT_2$ maintains directly after the control impulse occurs. This event leads to the turn-on losses and is typical for the hard-switching converters.

Due to the absence of the control system, the power variations were performed by changing the phase shift angle ϕ in order to regulate the amount of the transported power and by changing the output resistance of the converters in order to have appropriate currents in the circuits. The 2000 Hz model could go down to 13% of the nominal supply power. While the 10000 Hz model loses the lossless switching already at 34 % of the supply power. When it comes to the DAB topology, the 2000 Hz showed impressive 7 %. Below this boarder the switches which are situated on the primary side lose the lossless turn-on of the current. The limit for the 10000 Hz DAB converter is 16 %.

At the boarder conditions some parameters of the passive elements were changed in order to see the possibilities of the extension of the lossless region. In case of the SAB topology the biggest influence has the output inductor, where a larger choke provides an extended lossless region. The leakage inductance has the similar influence. However, it influences a lot on the primary current because it has tendency to limit it. A decrease of the output capacitances did not bring any noticeable results. Moreover, it would not be possible if the circuit was implemented in the reality because it is hard to decrease the internal capacitance of the transistor.

Chapter 6

Conclusions

In this chapter a summary of the completed work are presented.

6.1 Results from present work

Two different topologies were closely investigated in this thesis. The studied topologies are the Single-active bridge dc/dc converter and the Dual-active bridge dc/dc converter. The both topologies were evaluated in Simulink at two different frequencies and both of them have shown impressive results. The aim of the work was to find a suitable converter for an offshore application which would fulfil such requirements as a lightweight transformer core and reduced semiconductor losses such as the switching losses in the transistors and the reverse recovery losses in the power diodes.

Both topologies have similar construction of the primary side which resulted in similar losses in these parts. At the nominal power level, the both topologies performed without any switching or reverse recovery losses on the primary side.

When it comes to the secondary side, the Dual-active bridge topology has a more complex structure. It consists of four diodes and four switches compared to only four rectifier diodes in the SAB topology. In spite of the fact that the secondary diodes carry the most part of the current, the switches have very important function. They take over the current from the power diodes, providing a turn-off without the reverse recovery losses which constitute the biggest part of losses in case of the SAB topology. This fact allows us to consider the DAB converter as a better topology in terms of efficiency.

Regarding the investigation of the topologies at the different frequencies, the 2000 Hz models have shown better efficiency than the 10000 Hz models. This can be explained by the increase of the frequency-dependent losses, such as the magnetic core losses and the reverse recovery losses. On the other side the weight of the magnetic components is significantly decreased.

All of the four converters could work with pretty much reduced power transfer and stay in the lossless region. However, both of the DAB converters performed better than the corresponding SAB models. In terms of the operating frequency, the 2000 Hz models could reach lower power supply levels. During the simulations, it was found out that some increase of the leakage inductance would extend the lossless region of the converters. On the other side, high inductance in the circuit limits the main current and, hence, decreases the amount of transmitted power. This fact makes it impossible to use the same amount of inductance at different power levels.

6.2 Future work

The results of the work have shown that the Zero-voltage switching family could be a good choice for an application where the input power is unstable but still a high efficiency is required. The used simulation pro-

Chapter 6. Conclusions

gram Simulink does not reproduce many physical processes and the obtained results are not very close to realistic. However, this work reveals the potential of such topology as the DAB converter. Nevertheless, a further investigation, in a more advanced simulator is required.

References

- [1] *Nanocrystalline Cut Cores Made of Vitroperm 500 for Transformers.*
- [2] W. Andreyckak, "Phase-shifted full-bridge, zero-voltage transition design considerations," Texas Instruments, Tech. Rep., 2011.
- [3] V. Beldjajev and I. Roasto, "Dual active bridge based isolation stage for power electronic transformer," Tallinn Technical University, Tech. Rep.
- [4] G. D. Demetriades, "Evaluation of different topologies for high-power dc-dc converters," Ph.D. dissertation, KTH, 2001.
- [5] M. Fazlali and M. Mobarrez, "Design, simulation and evaluation of two different topologies for the 2.4 mw 4/6 kv dc-dc fullbridge converter," Master's thesis, Chalmers University of Technology, 2012.
- [6] N. G. Hingorani, *Understanding FACTS*. IEEE PRESS, 1999.
- [7] L. Max, "Design and control of a dc collection grid for a wind farm," Ph.D. dissertation, Chalmers University of technology, 2009.
- [8] N. Mohan, T. M. Undeland, and W. P. Robbins, *POWER ELECTRONICS Converters, Applications and Design*. John Wiley and Sons, 2003.
- [9] D. R. Seyezhai, "Performance evaluation of modulation strategies for dual active bridge multiport dc-dc converter," *IOSR Journal of Engineering (IOSRJEN)*.
- [10] <http://www.ti.com/lit/ml/slup124/slup124.pdf>, Texas Instruments.
- [11] M. Uslu, "Analysis, design, and implementation of a 5 kw zero voltage switching phase-shifted full-bridge dc/dc converter based power supply for arc welding machines," Master's thesis, Middle East Technical University, 2006.
- [12] D. Van Hertem, M. Ghandari, and M. Delimar, "Technical limitations towards a supergrid -a european prospective," in *2010 IEEE International Energy Conference*.
- [13] B. York, "Toroid design (single layer)," lecture Slides UCSB.